Isotropic-Helicoidal Transition of Semiflexible Polymers Confined to a Spherical Surface

by

Wuyang Zhang

A thesis
presented to the University of Waterloo
in fulfilment of the
thesis requirement for the degree of
Master of Science
in
Physics

Waterloo, Ontario, Canada, 2009

AUTHOR'S DECLARATION

I hereby declare that I am the sole author of this thesis. This is a true copy of the thesis, including any required final revisions, as accepted by my examiners.

I understand that my thesis may be made electronically available to the public.

Abstract

A semiflexible polymer confined to a spherical surface is used as a basic model for understanding DNA conformation in restricted space. By means of Monte Carlo simulation for a bead-rod chain generated on a spherical surface, we find an ordered helicoidal phase at sufficiently high surface density and determine the critical density of the isotropic-helicoidal phase transition for various persistence lengths. We verify that the excluded volume effect is the key factor to cause the helicoidal state. In addition to Monte Carlo simulations, we utilize the model of wormlike chain with Onsager's excluded volume interaction and examine the Landau expansion of the free energy involving both the orientational and spatial order parameters. We also analytically figure out the critical density and transition gap for various ratios of persistence lengths of the polymer chain and the radius of spherical surface. The results from both simulation and analysis are consistent with each other.

Acknowledgements

I am very grateful to Professor Jeff Z. Y. Chen, for his patient supervision and encouragement. I also want to give thanks to my friends. Without them, I will not have motivation to complete my study.

Contents

List of Figures

Chapter 1

Introduction

1.1 Eukaryotic DNA Wrapped Around Histone

Animals, plants, protists, and fungi are eukaryotes, which are defined by the existence of cell nucleus in their cells. Eukaryotic cell is organized into a complex system, including nucleus, cytoplasm, and other organelles, enclosed within membranes. Among them the cell nucleus bound in nucleus envelope is the cell's information center, which stores most of the cell's genetic material, called chromosomes and provides the place where almost all DNA replication and RNA synthesis occur. Chromatin, which is packaged to be chromosome, consists of one or more long linear DNA molecules associated with proteins, such as histones. The functions of chromatin are to package DNA into a smaller volume to be stored in nucleus, to allow mitosis and meiosis of chromosome, and to assist to operate DNA replication and realize expression of genetic information. Hence, the conformation of DNA in chromatin is of importance to study, understand, and explain biological process and mechanism of chromosome genetics.

In 1974 Kornborg [15] and Olins et. al.[22] observed linear arrays of spherical particles, which are called as nucleosomes later, in DNA conformation of chromatin to verify that a chromatin is a flexibly jointed chain consisting of repeating nucleosomes. More recent works [20, 27] revealed the fine structure of a nucleosome that is made up by DNA, a negatively charged semiflexible biopolymer, wrapped around positively charged histone proteins (See Fig. 1.1). This complex configuration can help very long DNA molecules

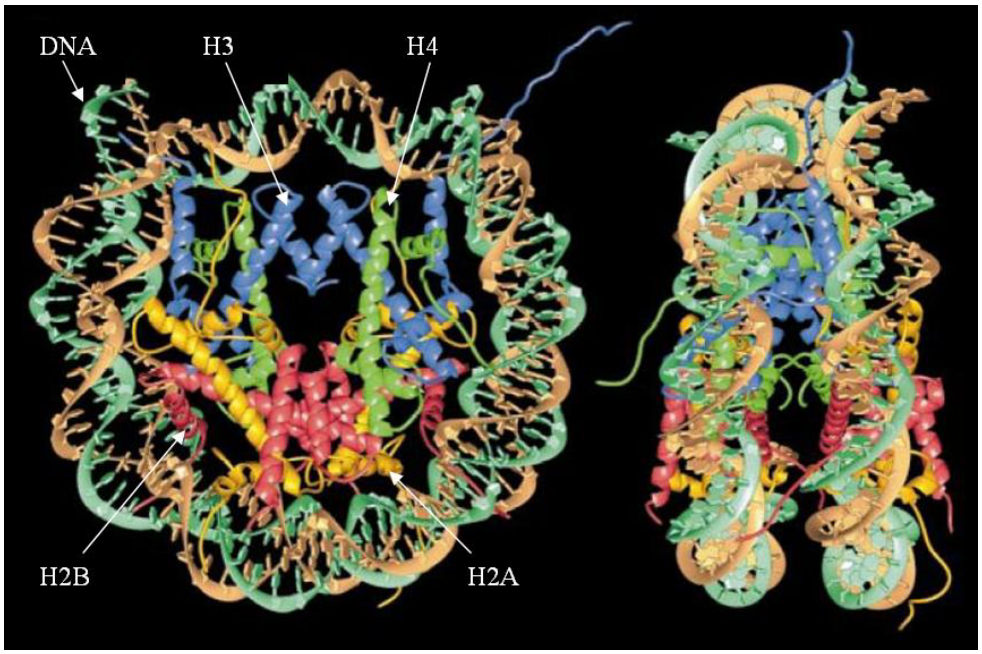

Figure 1.1: A nucleosome core particle is made up by DNA helicoidally wrapped around histone proteins consisting of four kinds of main protein chains: H2A, H2B, H3, and H4 [20].

be compressed to a high density in a relatively quite small nucleus. For example, approximately 1 meter of human DNA is compacted and stored in a nucleus of around 10 μm diameter, where the nucleosomes consist of DNA wrapped in about 2 circles around histone. Therefore, the structure and stability of nucleosomes, which is fundamental for understanding the biological behavior of chromosomes, has attracted waxing interest along with further investigation in genetics. Actually, the wrapping conformation of DNA around histone is relevant to the electrostatic attractions between DNA and histone, of course, as well as the electrostatic repulsion between any two monomers of DNA. Because the electrostatic interaction can be modulated by the salt concentration in a solution of histones, with some experiments on salt-induced DNA-histone complexation Yager and his co-workers [33] discovered that for some particular salt concentrations close to the physiological value of about $100mM$, DNA is tightly wrapped around histone. For small salt concentrations DNA can be partially dewrapped. A similar result could be referred in another theoretical investigation [16]. In our research we model DNA wrapped around histone proteins and investigate its conformation.

1.2 Bacteriophage DNA Packaged in Capsid

The conformation of DNA packaged in bacteriophage capsid is similar to that of DNA wrapped around histone. Bacteriophages as one of the simplest known creatures have made a lot of contributions to the development of molecule biology. The bacteriophage life cycle serves as one of the most fundamental model systems representing the propagation of organisms, and each stage of the cycle is equivalently significant for us to understand the whole process (See Fig. 1.2).

The detailed process of the bacteriophage life cycle could be described as following. In a host bacterium, DNA of bacteriophage is replicated according to the base pairs. After the bacteriophage assembles its protein capsid, the genome is inserted into the empty capsid driven by an ATP-consuming motor against the strong resistance, which comes from compressing the long polymer chain into the relatively small capsid. Large energies are stored in DNA after packaged. Then the newborn bacteriophage lyses the host cell, escapes, attaches to specific receptors on the surface of another host bacterium, and ejects DNA into the new host to reproduce its progeny. The energy restored in DNA

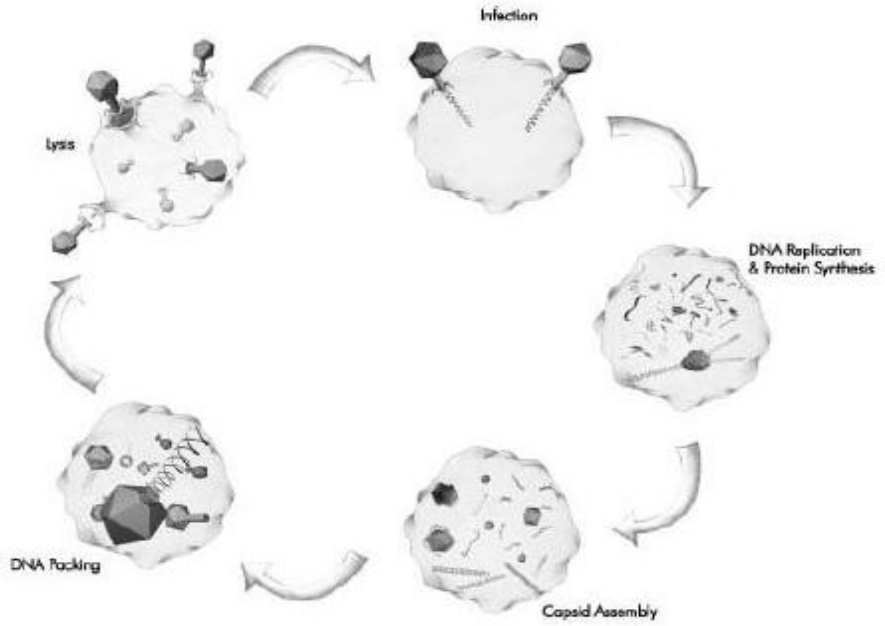

Figure 1.2: Bacteriophage life cycle consists typically of: DNA replication in a host bacterium, self-assembly of capsid proteins, DNA packaging into the empty capsid, lysis of the host bacterium, transport, absorption onto another host bacterium, and DNA ejection [25].

drives the ejection, because the bacteriophage can not use ATP to produce energy outside its host.

In the last century DNA replication and protein synthesis attracted a lot of attention. However, much recent progress in single molecule biophysics, x-ray crystallography, cryo-electron microscopy, etc. provide us the possibility to reveal and understand the precise manipulation of DNA during packaging and ejection. In the real-time single-bacteriophage packaging experiments [29] Smith et al. measured the force generated by the bacteriophage $\phi 29$ packaging motor when it packages a 6.6μm long DNA into a 54×42nm capsid [31]. This work showed the motor could overcome up to 57pN on average and become one of the most powerful molecular motors known to date. Another experiment by Evilevitch et al. [10] showed that the phage-λ could eject its DNA into a solution containing polyethylene glycol against an external osmotic pressure up to several tens of atmosphere, which reflects the forces during packaging. Besides the experiments, some theoretical investigations and computer simulations [25, 14] conclude that the DNA packaging and ejection force varies during the packaging or ejection process and depends on the ironic strength, phage identity etc.

The resistive force caused by the confinement of capsid compacts packaged DNA to ordered, typically tightly wound and spool-like, state in near-crystalline density. Almost 30 years ago an early x-ray diffraction experiment [9] by Earnshaw and Harrison revealed the packaged DNA to be organized into many circular rings to form several layers concentric to the shell of capsid and the distance between strands was around 2.8nm. Another experiment by Richards et al. [26] showed that DNA keeps close to the capsid boundary and has a circumferential orientation. More succeeding experimental evidences implied some potential models of DNA arrangement in capsid, including coaxial spool, concentric spool, folded coaxial spool, folded toroid, and so on. Recently, Cerritelli et al. [5] discovered the ordered state of packaged DNA anew when they investigated the encapsulated confirmation of bacteriophage T7 DNA by cryo-electron microscopy. Furthermore, they also found that the conformation is close to the coaxial spool-like model with several layers of coaxial spools, which are parallel to each other and perpendicular to the axis of the tail of the bacteriophage. Some other experiments of phage T4 [23] and P22 [35] showed similar results as well (See Fig. 1.3). Because of the stiffness and unpenetrable property of DNA, it tends to circle close to the capsid shell

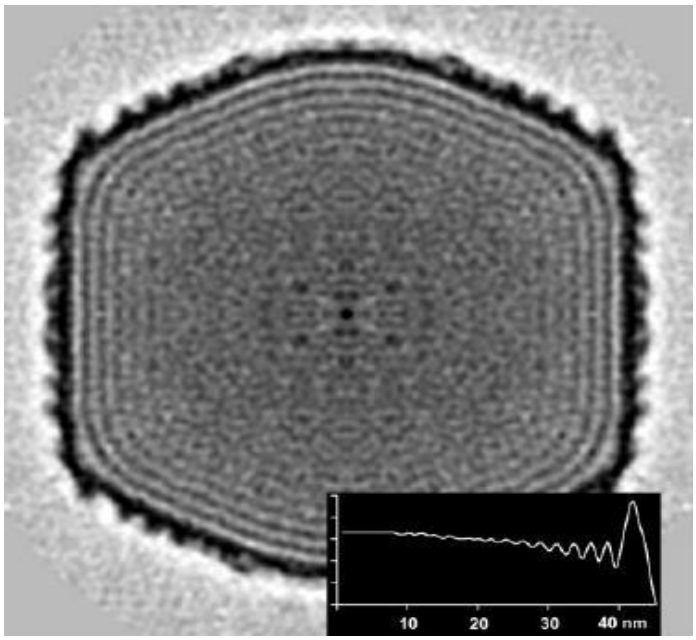

Figure 1.3: DNA of bacteriophage T4 is shown to be packaged in a highly condensed set of rings concentric to the capsid shell by means of cryo-electronic microscopy and image reconstruction techniques [23].

and keep in coaxial spools so as to hold the minimum bending energy.

Based on the evidence that the packaged DNA keeps close to the capsid shell [29], a fundamental and simplified two dimensional model could be considered as DNA confined onto a spherical surface.

1.3 Polymer Chain Confined to a Spherical Surface

The conformations of DNA wrapped around histone or packaged in a capsid can be illustrated by a simplified model, which is a semiflexible polymer chain, characterized by its persistence length and excluded volume, confined to a spherical surface, characterized by its radius. The purpose in studying this model of polymer systems is to find the re-

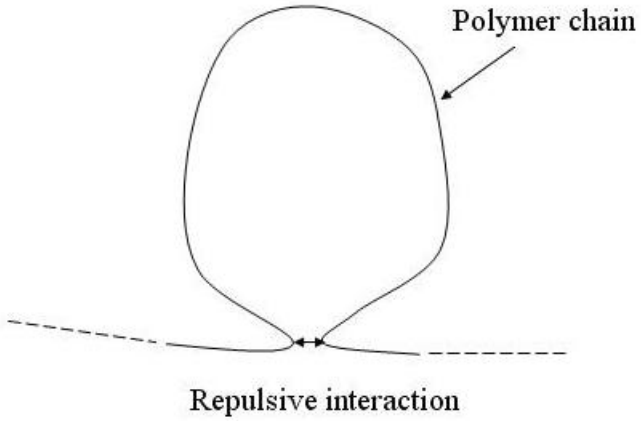

Figure 1.4: The long-range interaction comes from two monomers far away from each other along the chain, but typically in short range in space [12].

lationship between the physical properties and the monomer mutual interaction, without any concern about the exact chemical and structural details of a particular polymer.

1.3.1 Long- and Short-Range Interaction

There are two basic types of the monomer-monomer interactions in a polymer chain [12]: one is from neighboring or nearby monomers along the chain. We call it short-range interaction, which represents the connectivity constraints including the stiffness of the polymer chain. The other is long-range interaction, which comes from the monomers far away from each other along the chain, but typically in short range in space. Here the phrase "long range" does not refer to the force range of the monomers' mutual interaction, but means the long contour distance between the two interacting monomers (See Fig. 1.4), which contrasts with the short-range interaction associated with the connectivity.

1.3.2 Persistence Length

If the monomer-monomer short-range interaction behaves as some kind of stiffness, the polymer chain is called semiflexible. The persistence length, at which the polymer chain appears to be stiff, is used to quantify the stiffness. Usually, a general polymer chain is treated as a continuous curve $\boldsymbol{r}(\tau)$ and the stiffness is defined from the bending energy:

$$V_B = \frac{1}{2}\varepsilon \int_0^L \left| \frac{\partial \boldsymbol{u}(\tau)}{\partial \tau} \right|^2 d\tau = \frac{1}{2}\varepsilon \int_0^L |\ddot{\boldsymbol{r}}(\tau)|^2 \, d\tau \tag{1.1}$$

where τ is the contour length of polymer chain and $\boldsymbol{u}$ is defined as the unit tangent vector:

$$\boldsymbol{u}(\tau) = \dot{\boldsymbol{r}}(\tau) = \frac{d\boldsymbol{r}(\tau)}{d\tau} \tag{1.2}$$

as Saitô, Takahashi, and Yunoki [28] discussed. If the polymer chain is embedded in D spatial dimensions, the persistence length is defined in the tangent correlation function: [21, 13]

$$< \boldsymbol{u}(\tau) \cdot \boldsymbol{u}(\tau') >= e^{-|\tau - \tau'|/l_p} \tag{1.3}$$

where the persistence length $l_p = 2\beta\varepsilon/(D-1)$ which is reduced to $l_p = 2\beta\varepsilon$ for the 2 dimensional system. Here ε is the bending penalty in the bending energy and $\beta = 1/kT$. Polymer chain appears stiffer with longer persistence length.

1.3.3 Excluded Volume Effect

The long-range interaction in polymer system usually refers to the excluded volume effect, which behaves as the repulsive tendency between any two monomers close enough even though far away along the chain (See Fig. 1.4). Because of the excluded volume effect, polymers can form an anisotropic phase at high density. Onsager [24] originally introduced the idea that the isotropic-anisotropic transition is driven entropically and treated the repulsive interaction, i.e. excluded volume effect, as a key factor. At high density when the molecules are close to each other on average, because of the excluded volume interaction, rigid molecules tend to align in order to increase more accessible free volume. The greater entropy obtained from the additional free volume could compensate for the loss of orientational disorder.

Based on Onsager's Theory, we express the excluded volume effect as Onsager-like interaction in free energy of polymer chain:

$$v \iiint \rho(\boldsymbol{r}, \boldsymbol{u})\rho(\boldsymbol{r}, \boldsymbol{u}') \, |\boldsymbol{u} \times \boldsymbol{u}'| \, d\boldsymbol{r}d\boldsymbol{u}d\boldsymbol{u}' \tag{1.4}$$

where $\boldsymbol{r}$ is the position of polymer segment and $\boldsymbol{u}$ is the unit tangent vector of polymer segment at $\boldsymbol{r}$. ρ is the segmental density distribution of polymer. The excluded volume v per segment of a persistence length could be estimated statistically as $v = l_p^2$ for two dimensional system. The Onsager-like interaction makes any two monomer close enough to each other tend to be parallel according to the factor $|\boldsymbol{u} \times \boldsymbol{u}'|$.

1.3.4 Previous Theory and Simulations of Polymer Chains Confined to a Spherical Surface

Understanding the physical mechanism of DNA conformation can help us realize and even master the artificial manipulation of DNA. As a result the model of polymer chain confined to a spherical surface has been widely used to investigate DNA conformations in recent years. Some theoretical works on the wrapping confirmation of polymer chain on a spherical or other curved surface were published recently [30, 18]. In Spakowitz and Wang's work [30], they used a formalism to study the statistical behavior of wormlike chain confined to a spherical surface and provide an expression of the mean square end-to-end distance for any value of total chain length, persistence length, and sphere radius. In the work of Lin et al. [18], they obtained some numerical solutions of polymer conformations with local geometrical quantities on cylindrical and ellipsoidal surfaces based on the principle of minimization of free energy. In such works, however, no order parameter was involved to macroscopically describe the order of wrapping conformations as well as the disordered-ordered transition. Besides, one important effect, the excluded volume interaction, was not considered either. In fact, the distance of approximately 3nm between packaged DNA strands [9] seems not negligible relative to the scale of capsid. Another work [4] on the computer simulation on polymer chains confined to spherical surfaces verified that the excluded volume effect does influence the polymer conformation.

1.4 Our Purpose and Organization of the Thesis

In this thesis, we focus on the configuration of semiflexible polymer chain confined to a spherical surface taking into account the excluded volume interaction. For the purpose of explaining the helicoidal conformation of polymer we pay attention to the orientational and spatial distribution of the polymer chain instead of the mean square end-to-end distance. Here we build the coordinates for this system as Fig. 1.5 shows, where $\boldsymbol{r}$ is the position of polymer segment relative to the center of sphere, $\boldsymbol{u}$ is the tangent vector of polymer segment at $\boldsymbol{r}$, and the Z-axis is set to be the symmetric axis of the helicoidal conformation. Θ is used to represent the angle between Z-axis and the position vector $\boldsymbol{r}$ and θ is the angle between the azimuthal direction $\hat{\boldsymbol{\Phi}}$ and tangent vector $\boldsymbol{u}$. Then we define the order parameters according to the definition of two angles θ and Θ along the chain $\boldsymbol{r}(\tau)$:

$$\sigma = < \cos 2\theta > = < 2\cos^2\theta - 1 > \tag{1.5}$$

$$\eta = < P_2(\cos\Theta) > = < \frac{3\cos^2\Theta - 1}{2} > \tag{1.6}$$

where σ is the orientational order parameter and η is the spatial order parameter. The definitions of parameters come from the expansion of density distribution in the bases $P_n(\cos\Theta)\, e^{im\theta}$ on the spherical surface (See Appendix C for details). The average $< \cdots >$ is taken over the density distribution of polymer chain on the spherical surface.

The configuration of polymer chain confined to a spherical surface is determined by the balance controlled by the scale of sphere, the total contour length, the persistence length, and the excluded volume of polymer chain. We could imagine that the polymer chain would be in a disordered state in the limit of large sphere, short length, absolute flexibility, and tiny excluded volume, because of the abundant degrees of freedom . On the other hand, the polymer chain should be confined into an ordered state as mentioned before about DNA conformations [33, 23]. In this thesis we call the disordered and ordered state as isotropic and helicoidal phase respectively (See Fig. 1.6) and investigate how these parameters determine the order and phase transition by means of computer simulation and theoretical analysis. In Chapter 2 we first present the computer simulations on both orientational and spatial order parameters as well as the phase transition for the bead-rod model. Then, in Chapter 3, we theoretically analyzed the Landau ex-

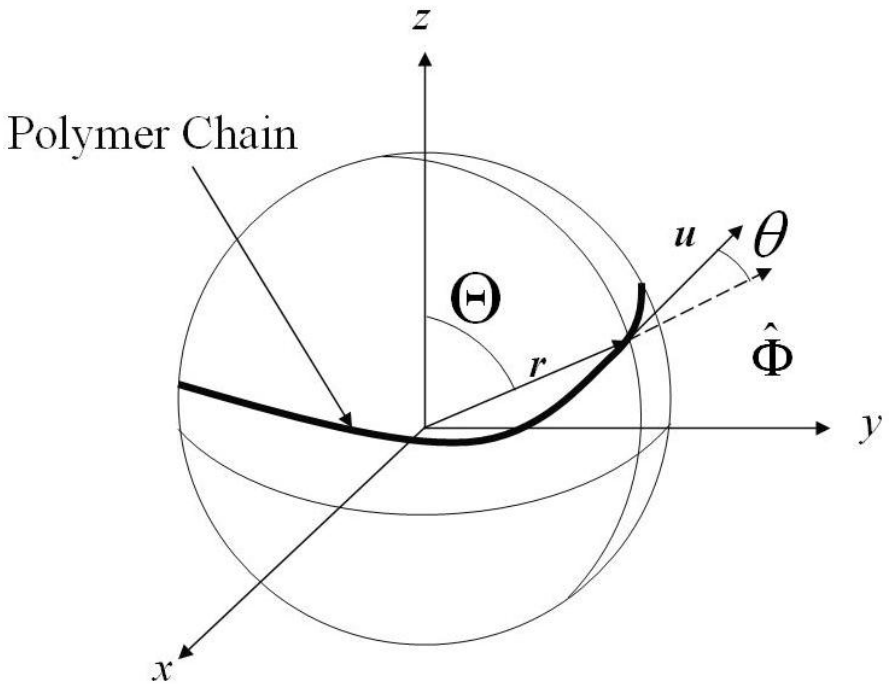

Figure 1.5: Definition of coordinates for a polymer chain on a spherical surface: $\boldsymbol{r}$ is the position of polymer segment according to the center of sphere, $\boldsymbol{u}$ is the tangent vector of polymer segment at $\boldsymbol{r}$, Θ is the angle between Z-axis and the position vector $\boldsymbol{r}$, and θ is the angle between $\hat{\boldsymbol{\Phi}}$ and tangent vector $\boldsymbol{u}$.

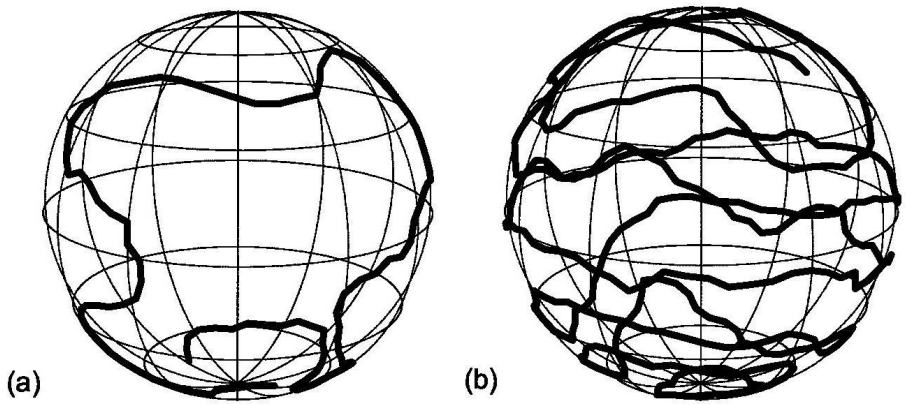

Figure 1.6: (a) The isotropic phase and (b) the helicoidal phase can be illustrated by the typical configurations from our simulation. The orientational order can be found at the helicoidal phase comparing to the isotropic phase.

pansion of the free energy to study the stable configuration and the isotropic-helicoidal phase transition for a wormlike chain confined to a spherical surface.

1.5 Theoretical Models Used in Our Research

Chainlike models of polymer molecules are widely used in polymer configurational statistics, where we consider various methods of approximation based on either physical origin or numerical nature. In our research, we use the bead-rod model in the computer simulation and the wormlike chain model in theoretical analysis respectively.

1.5.1 Freely-jointed Chain and Bead-rod Model

A freely-jointed chain is the simplest model to describe a polymer. It assumes a polymer as a random walk and the bond length is fixed on l. Angles between two neighboring

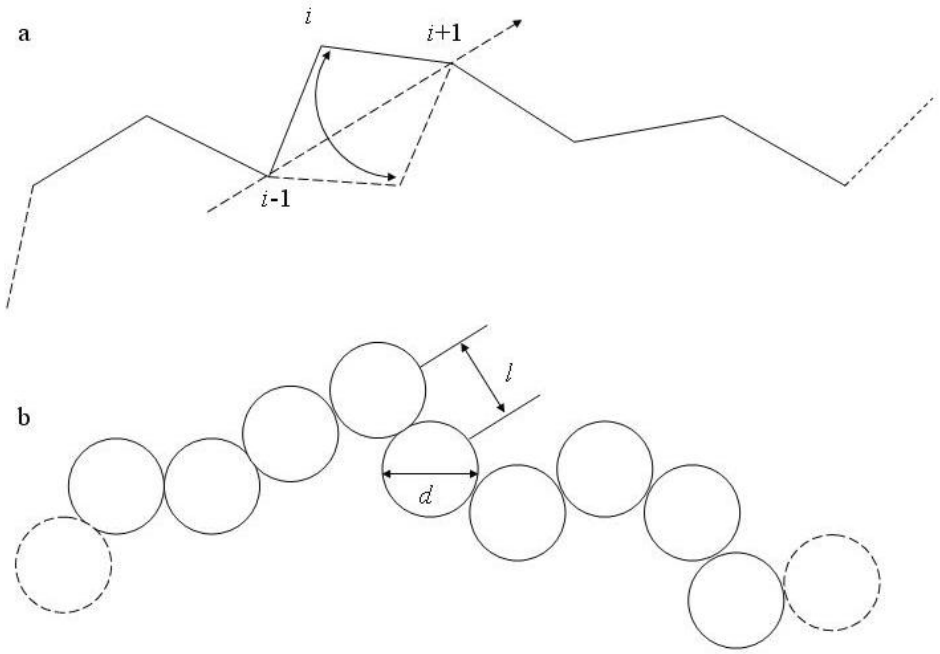

Figure 1.7: (a) A freely-jointed chain assumes a polymer as a random walk. Each node rotates around the axis connecting its two nearest-neighbors. (b) In the bead-rod model, each node is treated as a bead of diameter d.

bonds are not restricted. When the node moves, it has only one degree of freedom and rotates around the axis connecting its two nearest-neighbors (See Fig. 1.7.a). If the excluded volume should be considered, each node is treated as a bead of nonzero diameter. This is the bead-rod model or pearl necklace model [2] (See Fig. 1.7.b). In our research we also involve the bending energy in the bead-rod model to simulate a semiflexible polymer chain.

1.5.2 Wormlike Chain Model

A freely rotating chain, in which the bond lengths are fixed on l and the bond angles are fixed on θ, is developed from freely-jointed chain. The wormlike chain, which is used to

describe a semiflexible polymer, is the continuous model generated from discrete freely rotating chain by taking the limit $l \to 0$, $n \to \infty$, $\theta \to \pi$ and keeping the total contour length $L(= nl)$ constant [34, 12]. The persistence length l_p represents the length scale at which the wormlike chain appears to be stiff. Therefore, if we take the limit $l_p/L \to 0$, which means the contour length is much greater than the persistence length, the stiffness can be ignored and the chain becomes an absolutely flexible one. On the opposite limit, $l_p/L \to \infty$, the chain is stiff and reduces to a rigid rod.

In a word, the wormlike chain, described by a continuous curve, is a simple but useful model interpolating between the flexible and rigid limits and demonstrating the configurational properties of semiflexible polymers. In our analytic work, we use the wormlike chain model to simulate DNA molecules.

Chapter 2

Computer Simulation

2.1 Monte Carlo Simulation Technique of Bead-rod Model

In this chapter we present the results of computer simulations. At the beginning of a Monte Carlo simulation, we generate a bead-rod model chain on a spherical surface of radius R with $N_b + 1$ beads of diameter d (See Fig. 1.7.b). The length of each bond is fixed at $l = 1$ when the chain is created.

During the Monte Carlo simulation, we try to randomly move a randomly selected bead to a new possible position on the surface so as to build a new configuration of polymer. For the two ending monomers, each individual motion becomes wiggling within a random angle, while each non-ending bead rotates around the axis connecting the two nearest-neighbor monomers. Each possible position for any monomer is confined on the spherical surface for the two dimensional system. Because each monomer must be restricted by the spherical surface and the bonds, the polymer chain does not have many degrees of freedom and might be trapped in a sharp local potential well during Monte Carlo simulation. To solve this problem we permit that the bond length can change a little, less than $0.05l$, during each move in order to add some more degrees of freedom to the polymer chain to help the chain escape from a local potential well more easily.

The acceptance of each move is evaluated according to the standard Metropolis algorithm: $\exp(-\beta\Delta U) > \xi$, where ξ is a uniform, random number between 0 and 1, and ΔU

is the change in the total energy of the system involved in the proposed move. The total energy U is given by:

$$U = V_B + \sum_{i=1}^{N_b-1} \sum_{j\geq i+2}^{N_b+1} V_E\left(\boldsymbol{r}_{ij}\right) \tag{2.1}$$

Here V_B is the bending energy, which shares the similar definition as the continuous polymer chain model [4]:

$$V_B = \frac{1}{2} \sum_{i=1}^{N_b-1} \varepsilon \left|\boldsymbol{u}_{i+1} - \boldsymbol{u}_i\right|^2 = \sum_{i=1}^{N_b-1} 2\varepsilon(1+\cos\theta_i)^2 \tag{2.2}$$

where $\boldsymbol{u}$ is the bond vector, i.e. $\boldsymbol{u}_i = \boldsymbol{r}_{i+1} - \boldsymbol{r}_i$, θ is the bond angle between any two consecutive bonds and ε is the bending penalty, which is related to the persistence length l_p by $l_p = 2\beta\varepsilon$ [13]. V_E is the hard-sphere potential:

$$V_E(\boldsymbol{r}_{ij}) = \begin{cases} 0 & \text{if} \quad \boldsymbol{r}_{ij} > d \\ \infty & \text{if} \quad \boldsymbol{r}_{ij} < d \end{cases} \tag{2.3}$$

where $\boldsymbol{r}_{ij} = \left|\boldsymbol{r}_i - \boldsymbol{r}_j\right|$ is the distance between two beads. The hard sphere potential guarantees that the polymer chain can not cross itself.

In our simulations in order to observe the order parameters of a semiflexible polymer chain with different persistence length at various density, we set $R = 20$, $d = 0, 1, 1.5$, and $\beta\varepsilon = 2, 4, 6, ..., 20$ and alter the number of bonds N_b in a range from tens to hundreds. The bond length l is approximately 1 on average during the simulation. Here we choose different diameter of beads to investigate the influence of bead's volume to the order.

N_b attempts to move are called as one Monte Carlo Step, in which each monomer is selected once on average. We find the bending energy V_B tends to be stable after 1×10^7 Monte Carlo steps, which represents the system reaches equilibrium. After initial 5×10^7 MCS (Monte Carlo Steps), chain properties have been evaluated every 100 MCS and averaged over 10^6 measurements, i.e. 10^8 MCS. A neighbor-list method [1] has been implemented in the algorithm in order to improve computation efficiency. For every measurement we evaluated the orientational and spatial order parameters:

$$\sigma = 2\left[\frac{1}{N_b}\sum_{i=1}^{N_b}\left(\frac{\boldsymbol{u}_i}{|\boldsymbol{u}_i|}\cdot\hat{\boldsymbol{\Phi}}_i\right)^2\right] - 1 \tag{2.4}$$

$$\eta = \frac{3}{2}\left[\frac{1}{N_b}\sum_{i=1}^{N_b}\left(\frac{\boldsymbol{r}'_i}{\left|\boldsymbol{r}'_i\right|}\cdot\hat{\boldsymbol{Z}}\right)^2\right] - \frac{1}{2} \tag{2.5}$$

defined for the discrete system according to the definition in Chapter 1 (Eqn. 1.5 and 1.6), where $\boldsymbol{r}'_i$ is the position of bond center, i.e. $\boldsymbol{r}'_i = (\boldsymbol{r}_{i+1} + \boldsymbol{r}_i)/2$. With the relation

$$\hat{\boldsymbol{\Phi}}_i = \frac{\hat{\boldsymbol{Z}} \times \boldsymbol{r}'_i}{\left|\hat{\boldsymbol{Z}} \times \boldsymbol{r}'_i\right|} \tag{2.6}$$

we could describe the orientational order parameter as

$$\begin{aligned} \sigma &= 2\left[\frac{1}{N_b}\sum_{i=1}^{N_b}\left(\frac{\boldsymbol{u}_i}{|\boldsymbol{u}_i|}\cdot\hat{\boldsymbol{\Phi}}_i\right)^2\right] - 1 \\ &= 2\left[\frac{1}{N_b}\sum_{i=1}^{N_b}\left(\frac{\boldsymbol{u}_i}{|\boldsymbol{u}_i|}\cdot\frac{\hat{\boldsymbol{Z}} \times \boldsymbol{r}'_i}{\left|\hat{\boldsymbol{Z}} \times \boldsymbol{r}'_i\right|}\right)^2\right] - 1 \end{aligned} \tag{2.7}$$

The Z-axis, i.e. the symmetric axis, moves along with consecutively altered configuration during Monte Carlo simulation. Hence, for every measurement, we re-establish the Z-axis according to the assumption that the Z-axis makes the orientational order parameter maximum. For any configuration we wish to evaluate, we treat the orientational order parameter as a two-variable function of the spherical coordinates of the Z-axis' orientation and use the Limited Memory BFGS algorithm to accomplish the maximization and find the corresponding Z-axis.

BFGS stands for Broyden-Fletcher-Goldfarb-Shanno, four persons who first introduced the BFGS method to solve an unconstrained nonlinear optimization problem. BFGS method is derived from Newton's method in optimization. For a multi-variable function $f(\boldsymbol{x})$ and a given initial point $\boldsymbol{x}_0$, BFGS method iteratively provides points $\boldsymbol{x}_i$ ($i \geq 1$) from previous one $\boldsymbol{x}_{i-1}$ along with the gradient direction until the function reaches its local minimum, where the gradient is 0. BFGS method is one of the most highly effective methods to locally minimize a function with multiple variables according to its gradient [3, 19]. In our simulation, we initially set the Z-axis to several different directions and choose the greatest local maximum to achieve the global maximization.

2.2 Orientational Order at Various Surface Densities

In this section, we show the relationship between the orientational order parameter and the surface density $\rho = N_b/4\pi R^2$ with a series of ten values of bending penalty $\beta\varepsilon =$

$2, 4, 6, ..., 20$ and a fixed sphere radius $R = 20$. In each case, we alter the number of bonds N_b to investigate the conformation of polymer chain at various surface density ρ. We would like to discuss the spatial order parameter later.

To obtain the influence of the excluded volume effect to the conformation, we measure the orientational order parameters σ for $d = 0$ without excluded volume effect and $d = 1, 1.5$ with excluded volume effect, respectively. We have to mention that, for the bead-rod model, the diameter d of each bead does affect the polymer conformation to some extend. However, for a 2D system, if the persistence length is much longer than the bead diameter, the excluded volume is primarily determined by the persistence length as $v = l_p^2$, where v is the excluded volume per segment of a persistence length. In this case, the influence of the hard sphere potential of each bead can be neglected and the bead-rod model works well to simulate a polymer chain as a continuous curve. In the opposite, if the bead diameter cannot be disregarded relative to the persistence length, the hard sphere potential for each bead must contribute to the excluded volume effect so as to influence the order parameters.

Here we show the figures (Fig. 2.1-2.5) to illustrate the orientational order parameter at various bead diameters and persistence lengths.

First, as Fig. 2.1-2.5 shows, for chains without excluded volume effect, i.e. $d = 0$, the orientational order parameter σ gradually vanishes at high surface density. This is because, without the excluded volume effect, the longer total contour length makes the polymer segments to occupy more possible orientations on the spherical surface (See Eqn. 1.3). However, if we involve the hard sphere potential for each bead, σ increases significantly at some critical density, which means the excluded volume interaction causes an ordered orientational distribution of segments.

Second, for the relatively short persistence length, say $l_p = 4$, i.e. $\beta\varepsilon = 2$ (See Fig. 2.1.(1)), we can find the different critical densities induced by the different bead diameters $d = 1$ and $d = 1.5$. For the larger diameter, i.e. $d = 1.5$, the transition takes place at a relatively smaller density. In addition, the order parameter σ for $d = 1.5$ is greater than that for $d = 1$ at the same density. All of these can be explained as that the larger diameter of beads induces the larger excluded volume.

Furthermore, if we set a longer persistence length, say $l_p \geq 12$, i.e. $\beta\varepsilon \geq 6$ (See

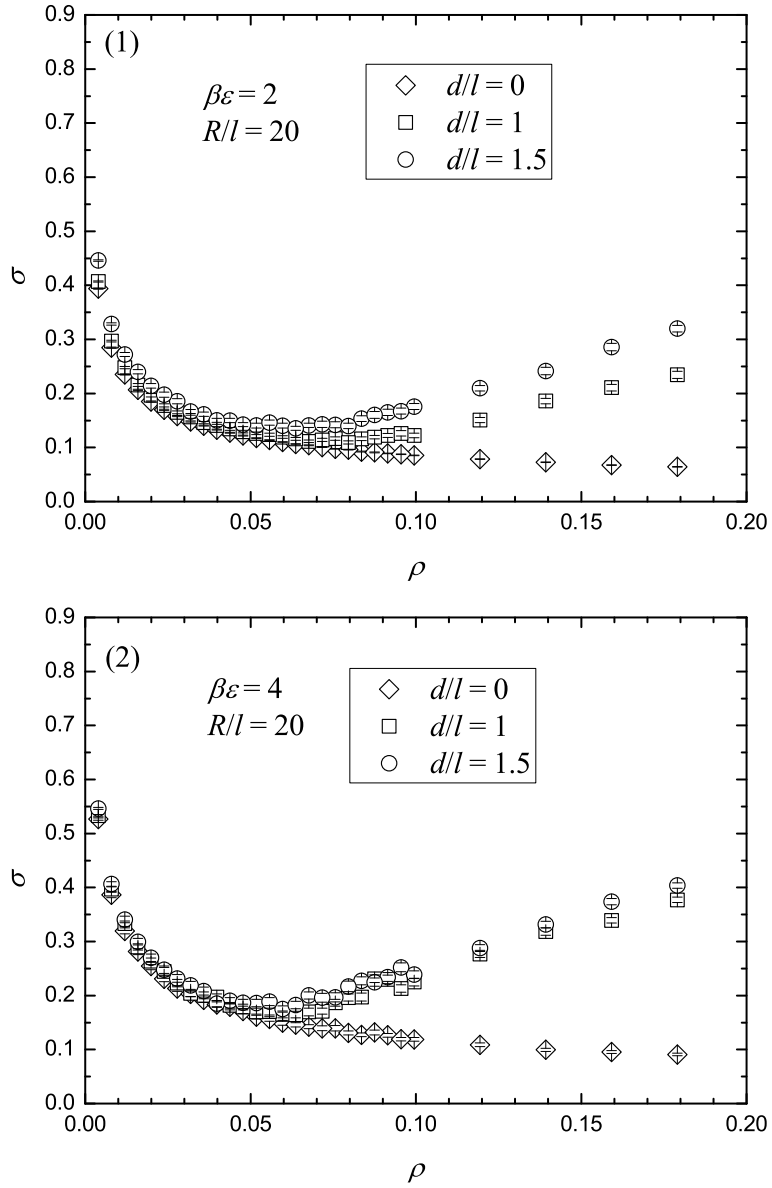

Figure 2.1: The orientational order parameter $\sigma =< \cos 2\theta >$ (Eqn. 2.7) versus the surface density $\rho = N_b/4\pi R^2$ for $d = 0, 1, 1.5$, $\beta\varepsilon = 2, 4$ and $R = 20$.

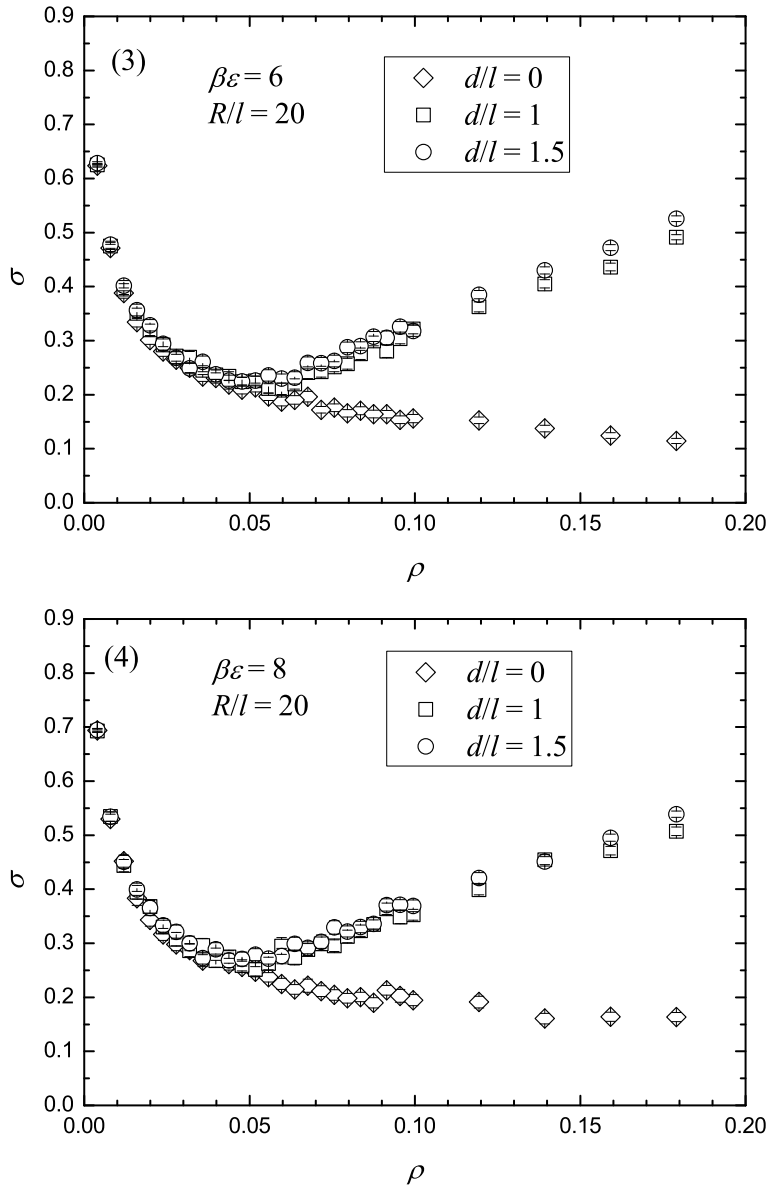

Figure 2.2: The orientational order parameter $\sigma =< \cos 2\theta >$ (Eqn. 2.7) versus the surface density $\rho = N_b/4\pi R^2$ for $d = 0, 1, 1.5$, $\beta\varepsilon = 6, 8$ and $R = 20$.

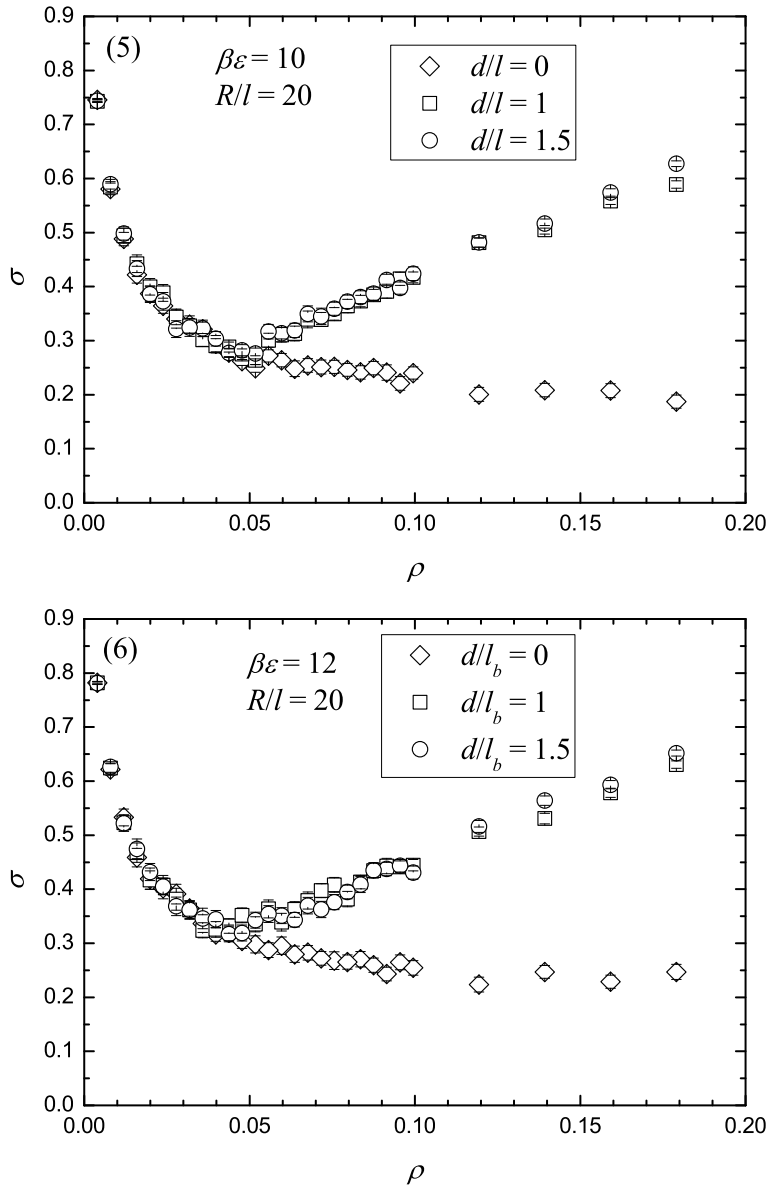

Figure 2.3: The orientational order parameter $\sigma =< \cos 2\theta >$ (Eqn. 2.7) versus the surface density $\rho = N_b/4\pi R^2$ for $d = 0, 1, 1.5$, $\beta\varepsilon = 10, 12$ and $R = 20$.

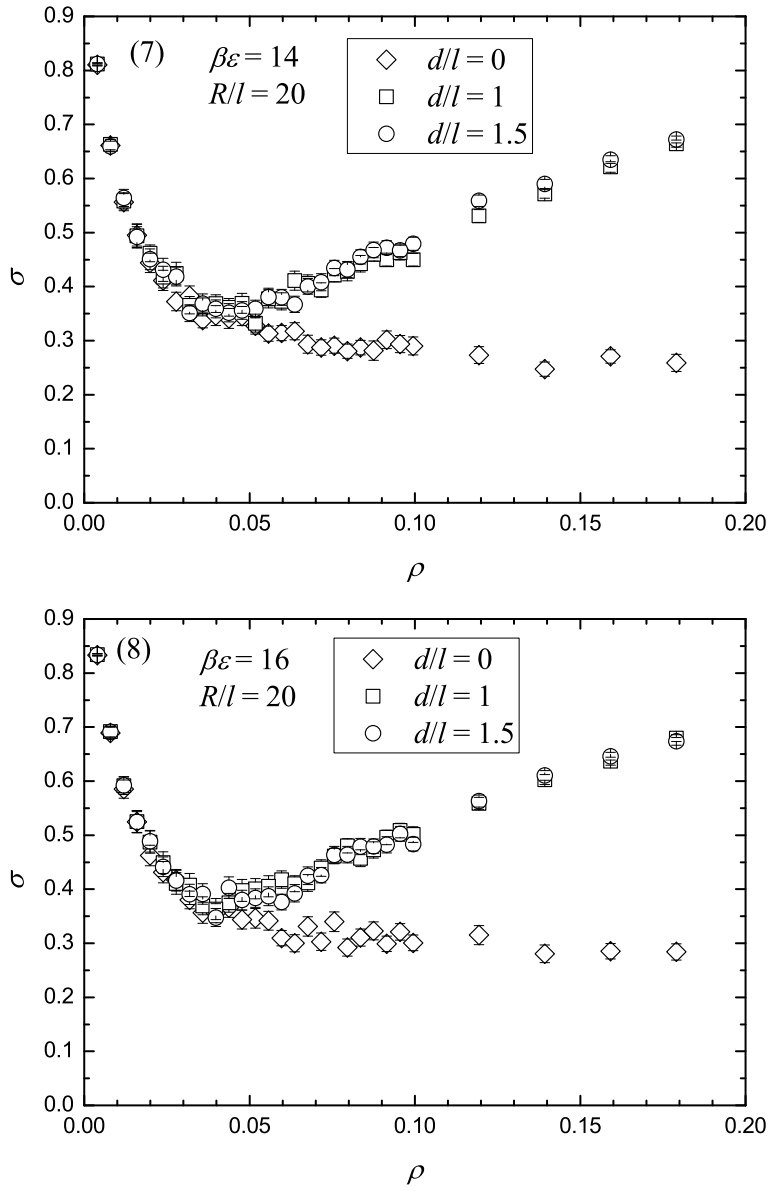

Figure 2.4: The orientational order parameter $\sigma =< \cos 2\theta >$ (Eqn. 2.7) versus the surface density $\rho = N_b/4\pi R^2$ for $d = 0, 1, 1.5$, $\beta\varepsilon = 14, 16$ and $R = 20$.

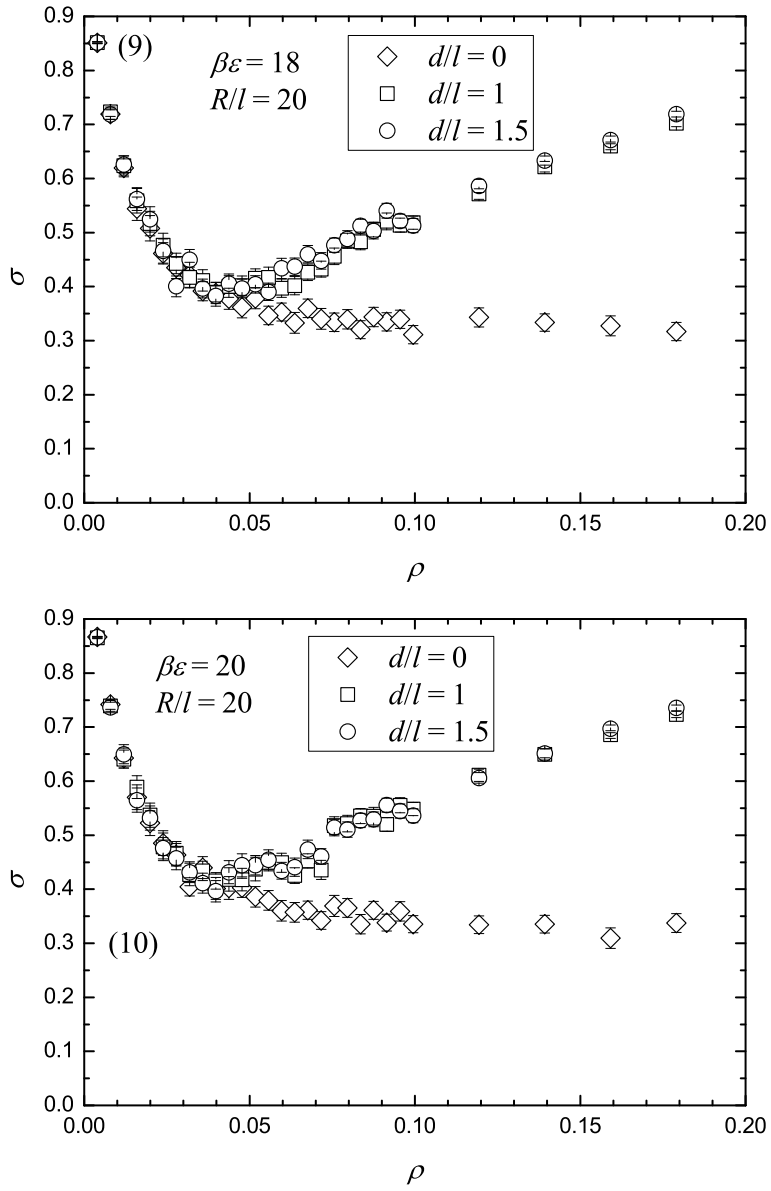

Figure 2.5: The orientational order parameter $\sigma =< \cos 2\theta >$ (Eqn. 2.7) versus the surface density $\rho = N_b/4\pi R^2$ for $d = 0, 1, 1.5, \beta\varepsilon = 18, 20$ and $R = 20$.

Fig. 2.2-2.5), the difference of order parameters induced by various bead diameter decreases or even vanishes. This verifies the influence of bead diameters to the order parameters can be weakened or even canceled for stiffer polymer chains. In other words, for a polymer chain with sufficiently long persistence length embedded in 2 dimensions, the contribution of the bead volume to total excluded volume can be neglected and the excluded volume is mainly determined by the persistence length.

Finally, the orientational order parameters for all different bead diameters are close to each other at low surface density in each case. The reason is that the total contour length of polymer chain is too short to wrap the chain around the sphere so as that the excluded volume effect can not take place. We would like to utilize the spatial distribution to indicate such conformations of short chains in Section 2.5. To represent the orientational order associated with the excluded volume effect, we define the effective orientational order parameter $\Delta\sigma = \sigma\,[d\,(\neq 0)] - \sigma\,[d = 0]$, which will be introduced later. Actually the "order" for short chains comes from the stiffness of polymer chain, because the short total contour length makes the orientations of all the bonds strongly correlated to each other by the stiffness (See Eqn. 1.3). Of course, for chains with the same persistence length, shorter one has greater order. In this case a polymer chain resembles a rigid rod. Therefore, we find that, at the same low density, the order parameter for the chain with longer persistence length is greater. This means stiffer polymer chains have greater orientational order.

2.3 Orientational Ordering and Helicoidal Conformation

To obtain the orientational order associated with the excluded volume effect, we define the effective orientational order parameter as $\Delta\sigma = \sigma\,[d\,(\neq 0)] - \sigma\,[d = 0]$, and then plot the figures (Fig. 2.6-2.10) for the same cases in Fig. 2.1-2.5.

In the figures (Fig. 2.6-2.10), the data for open symbols are measured within 10^8 MCS and those shown as symbols with a cross in the center are estimated over 10^9 MCS, which could provide more accurate result. These figures show us the relationship between the orientation order and the surface density. At the low surface density, the order parameter is close to zero, which represents the disordered isotropic phase (See

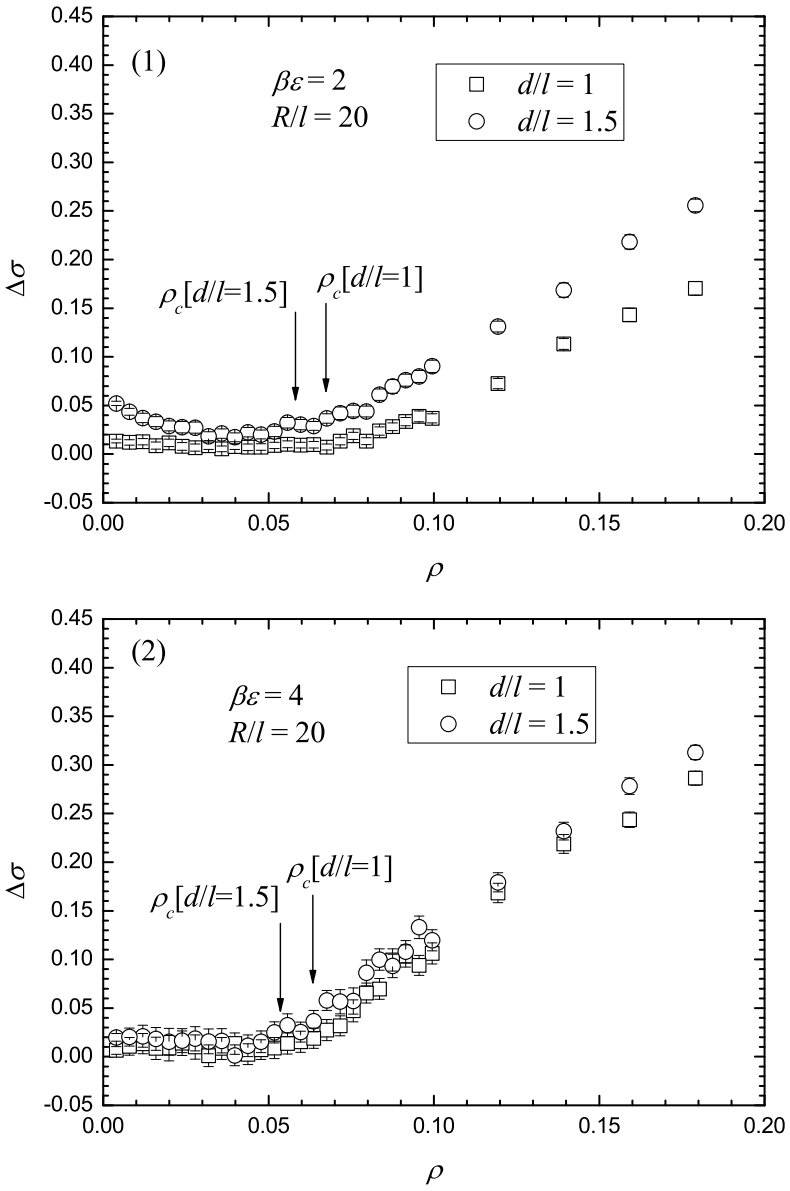

Figure 2.6: The effective orientational order parameter $\Delta\sigma = \sigma[d] - \sigma[d = 0]$ versus the surface density $\rho = N_b/4\pi R^2$ for $\beta\varepsilon = 2, 4$ and $R = 20$.

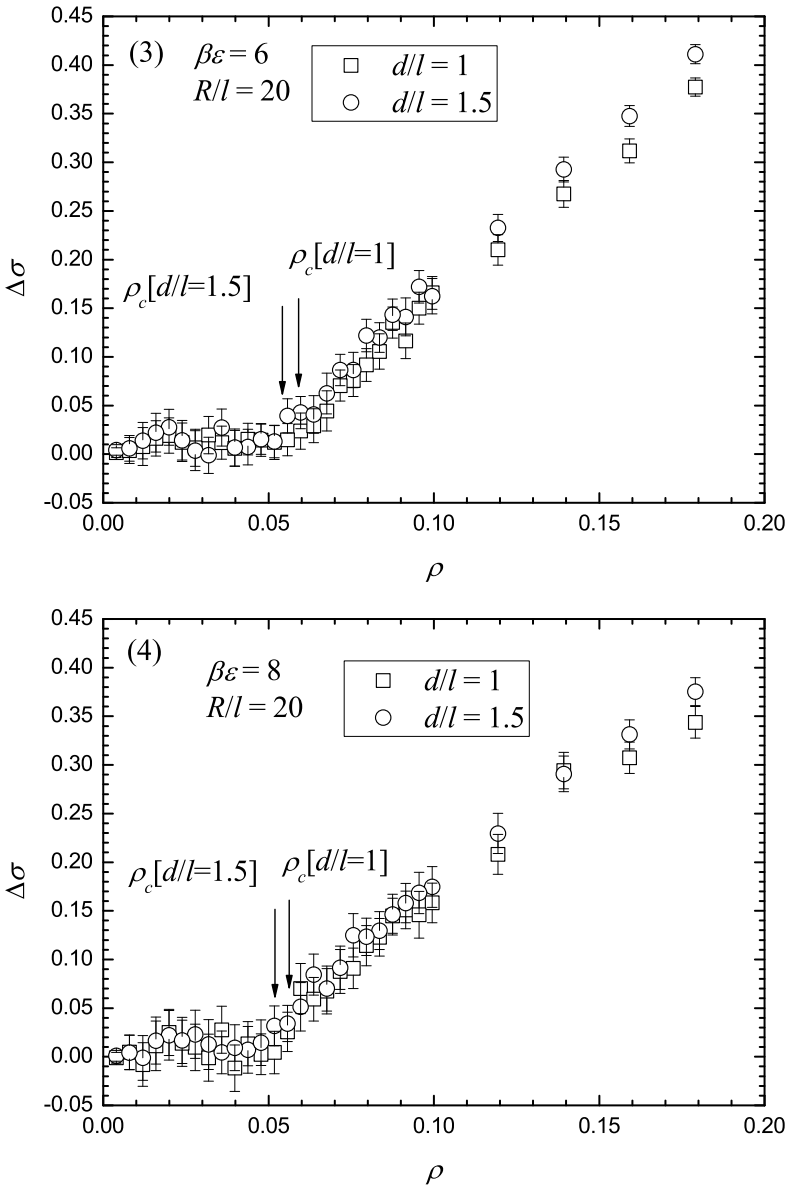

Figure 2.7: The effective orientational order parameter $\Delta\sigma = \sigma[d] - \sigma[d = 0]$ versus the surface density $\rho = N_b/4\pi R^2$ for $\beta\varepsilon = 6, 8$ and $R = 20$.

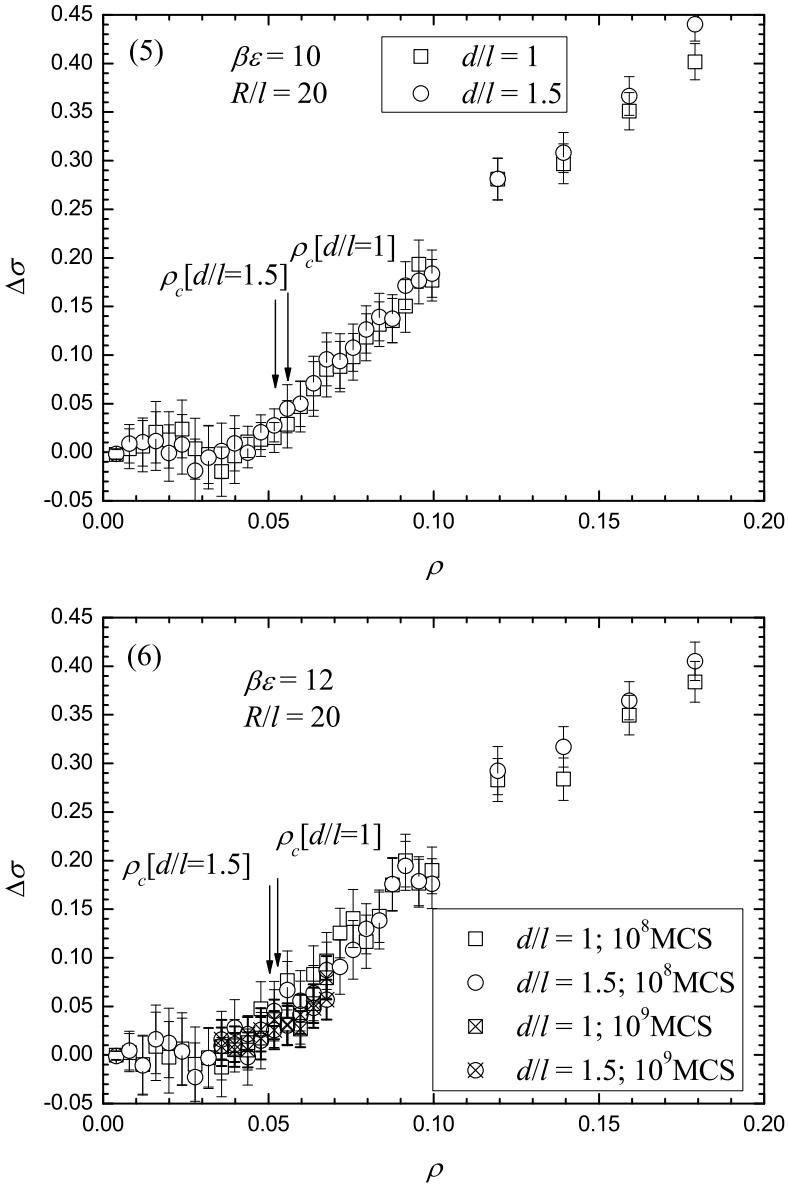

Figure 2.8: The effective orientational order parameter $\Delta\sigma = \sigma[d] - \sigma[d = 0]$ versus the surface density $\rho = N_b/4\pi R^2$ for $\beta\varepsilon = 10, 12$ and $R = 20$.

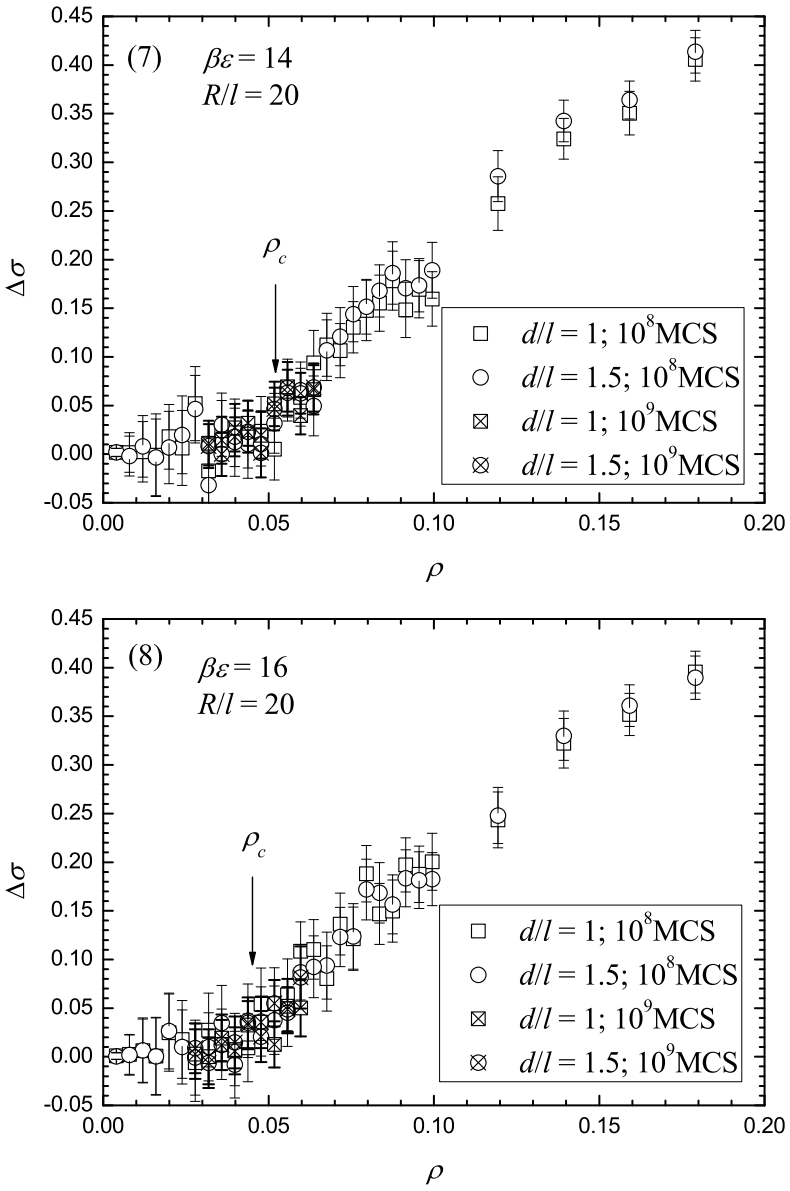

Figure 2.9: The effective orientational order parameter $\Delta\sigma = \sigma[d] - \sigma[d = 0]$ versus the surface density $\rho = N_b/4\pi R^2$ for $\beta\varepsilon = 14, 16$ and $R = 20$.

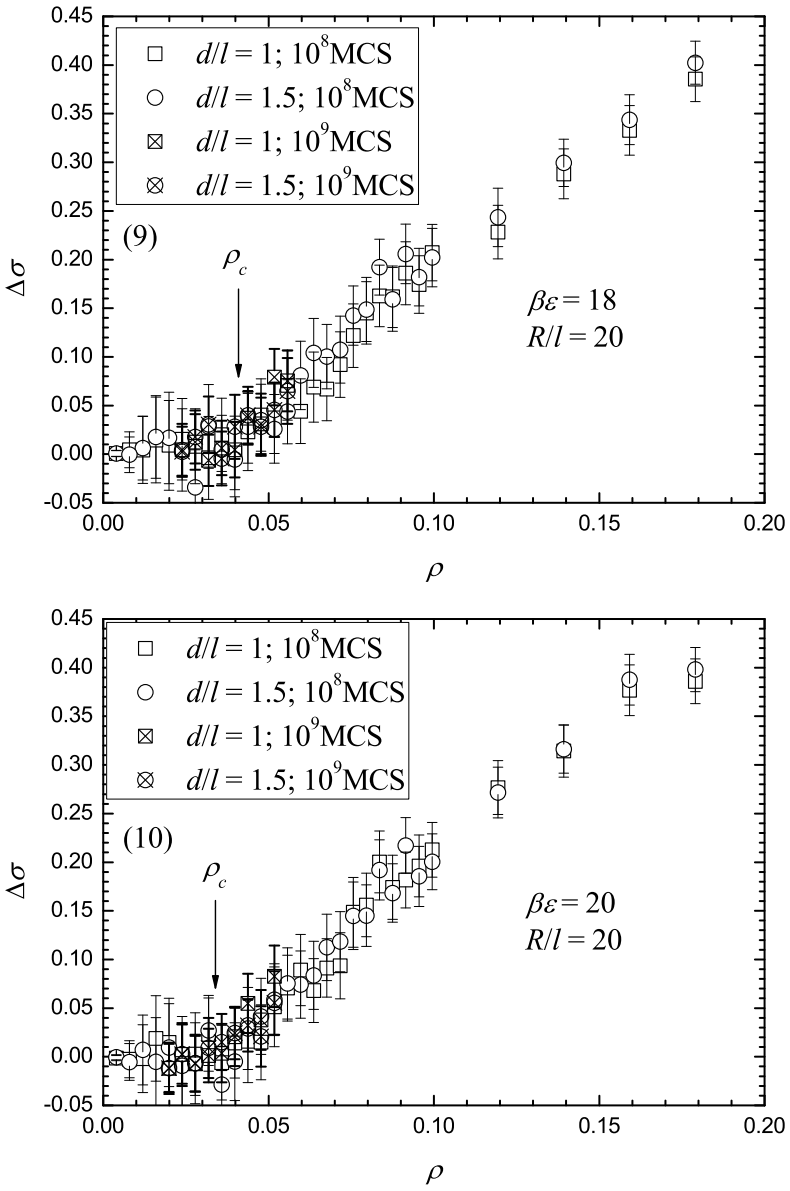

Figure 2.10: The effective orientational order parameter $\Delta\sigma = \sigma[d] - \sigma[d = 0]$ versus the surface density $\rho = N_b/4\pi R^2$ for $\beta\varepsilon = 18, 20$ and $R = 20$.

Fig. 1.6.a). Meanwhile, if the surface density is higher than the critical density ρ_c, the nonzero order parameter unveils the ordered configuration, which is called as helicoidal phase (See Fig. 1.6.b). The data verifies the assumption, which has been mentioned in Chapter 1, that the orientational configuration could become ordered or disordered according to the surface density. And the helicoidal state survives at high density. A previous simulation work [4] showed a similar figure of a polymer chain helicoidally wrapped around a sphere like Fig. 1.6.b.

According to the figures (Fig. 2.6-2.10) about the effective orientational order parameter, we estimate the critical densites ρ_c visually according to the intersection of the curve representing nonzero order parameters and the line for $\sigma = 0$.

2.4 Phase Diagram

The isotropic-helicoidal phase transition takes place at sufficiently high surface density for a polymer chain confined to a spherical surface. Based on the figures on effective orientational order parameters (Fig. 2.6-2.10), we can estimate the values of critical surface density ρ_c for each case and draw a phase diagram, in which the critical density is plotted as a function of l_p/R, the ratio of the persistence length and sphere radius (Fig. 2.11.a).

Here we use the bead-rod model to simulate a general polymer chain, i.e. a continuous curve like a wormlike chain, which does not have beads and bonds within its structure. Usually the bead-rod model with infinitely tiny beads and short bonds could be treat as a perfect symbolization of a wormlike chain within the continuous limit. In this case the more physically meaningful parameter associated with surface density is defined by the number of segments instead of bonds. A segment is a part of polymer chain within a persistence length. So the number of segments for a polymer chain with a total contour length L is $N = L/l_p$. With the relationship $L = N_b l$, where N_b is the number of bonds and l is the bond length as defined before, the segmental density can be described by:

$$\tilde{\rho} = \frac{L/l_p}{4\pi R^2} = \frac{N_b l}{4\pi R^2 l_p} \tag{2.8}$$

The ratio of the total excluded volume and the total space volume is an important parameter to estimate whether a polymer chain is at isotropic or helicoidal phase. For

a wormlike chain embedded in 2 dimensions, the excluded volume per segment of a persistence length is $v = l_p^2$. So the ratio could be expressed as:

$$n = \frac{Nv}{4\pi R^2} = \frac{N_b l l_p}{4\pi R^2} \tag{2.9}$$

According to the dimensionless parameter n, we plot another phase diagram (Fig. 2.11.b), which is more convenient to be compared with the result of theoretical analysis in Chapter 3.

We divide the phase diagram (Fig. 2.11.b) into three regions according to the value of l_p/R to discuss them respectively. In region I for $l_p/R < 1.0$, the hard-sphere potential in the bead-rod model becomes a significant part of the excluded volume because of the relatively short persistence length. Furthermore, for extremely short persistence length, almost all of the excluded volume comes from the hard-sphere potential so that the total excluded volume per polymer chain could be written approximately as $N_b dl$, where N_b is the number of bonds, d is the bead diameter and l is the bond length. Therefore, the ratio of total excluded volume and total space volume could be reduced to $N_b d/R^2$. So, for small l_p/R, N_b/R^2 as a function of l_p/R is approximately constant and $N_b l_p/R^2$ of l_p/R tends to be linear as what Fig. 2.11.a and Fig. 2.11.b show and the greater diameter d induces lower critical density.

In region II for $1 < l_p/R < 1.6$, the persistence length is long enough to weaken the contribution of the bead volume to the excluded volume. If we neglect the influence of hard-sphere potential completely, the ratio of total excluded volume and total space volume is definitely n in Eqn. 2.9. Its critical value for the polymer chain confined to a plane is constant [6, 7]. The spherical surface approaches a plane by taking the limit $l_p/R \to 0$, which will be discussed in Chapter 3. With longer persistence length in region II, i.e. $1 < l_p/R < 1.6$, the critical value of n, is approaching to critical n for the polymer chain on a plane.

For the longer persistence length $l_p/R > 1.6$, called region III, the critical value of n decreases for larger l_p/R. This decrease comes from the inhomogeneous spatial distribution of polymer chain on the spherical surface. We will talk about this in the chapter of theoretical analysis later.

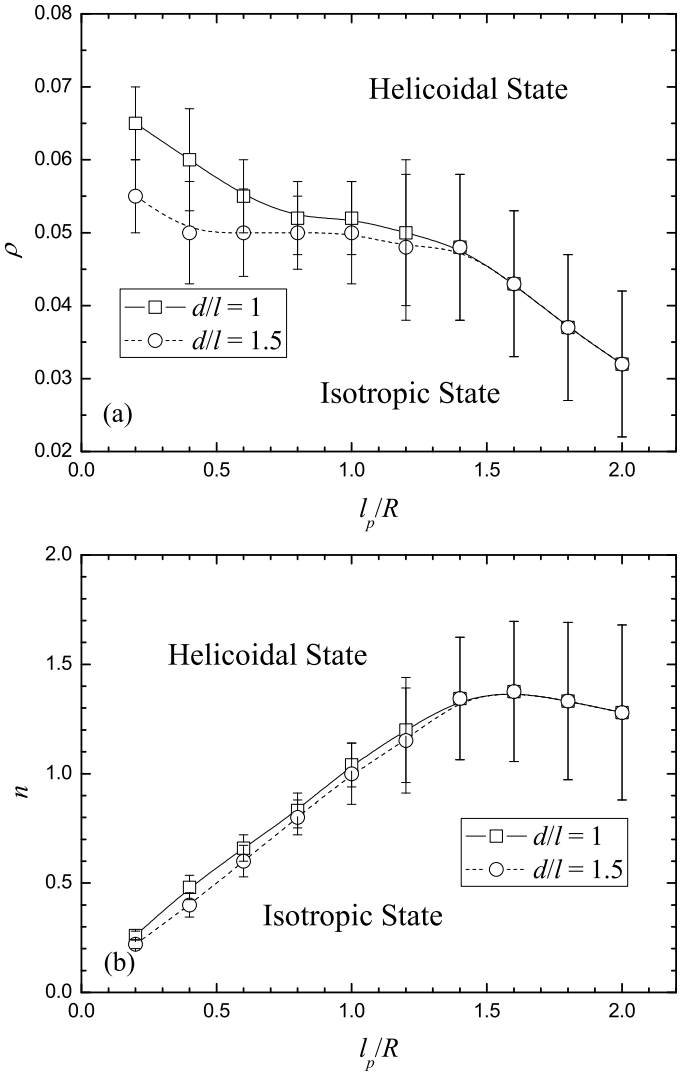

Figure 2.11: (a) The critical surface density $\rho = N_b/4\pi R^2$ and (b) The critical value of $n = N_b l l_p/4\pi R^2$ is plotted as a function of l_p/R, the ratio of the persistence length and sphere radius.

2.5 Spatial Configuration

During the Monte Carlo simulations, we also measured the spatial order parameter η at various densities besides the orientational order parameter in Fig. 2.1-2.5. Both the orientational and spatial order parameters depend on the symmetrical axis, i.e. Z-axis (See Eqn. 2.7 and 2.5). Fig. 2.12-2.16 show the same ten cases with various $\beta\varepsilon$ as Fig. 2.1-2.5 and Fig. 2.6-2.10.

First, at high density, say $\rho > 0.1$, the negative value of $\eta\,[d \neq 0] - \eta\,[d = 0]$ verifies that, at the helicoidal state, chains with excluded volume tend to occupy the positions near the equator in order to store less bending energy. Actually the polymer chain without excluded volume ($d = 0$) could not hold an orientational order and could also not form a helicoidal conformation so that the equator could not be defined or observed in this case.

Then, for chains with excluded volume ($d \neq 0$), the spatial order parameter decreases at even larger density ($\rho > 0.15$). The reason is that more and more beads, which can not overlap with each other because of the hard sphere potential, have to occupy the positions far from the equator so as that the spatial distribution approaches uniform.

Finally, to investigate the polymer conformation at low density, we also estimate the azimuthal dependence of spatial distribution, which can be illustrated by

$$< \cos\Delta\Phi >= \frac{1}{N_b}\sum_{i=1}^{N_b}\cos\left(\Phi_i - \Phi_M\right) \tag{2.10}$$

where Φ_i is the azimuth of i-th bond and Φ_M for the middle one. For a uniform distribution of Φ_i of bonds, $< \cos\Delta\Phi >= 0$. Otherwise, the polymer chain is not wrapped uniformly around the sphere. As Fig. 2.17-2.21 shows, at low density, the positive $< \cos\Delta\Phi >$ implies that the polymer chain is too short to wrap around the sphere but forms an arch on the surface. In this case, the polymer chain behaves like a rigid rod for orientational distribution. And for the spatial distribution, the chain with shorter persistence length is more flexible so as to be accepted with more probability as an arc of the small circle. In this case, Z-axis goes though the center of small circle which sets the polymer chain near one pole and generates a positive spatial order parameter. Meanwhile, at the same density, if we set longer persistence length to make the chain stiffer, the arc approaches a great circle of the sphere, because the great circle holds lowest curvature, and the spatial order parameter η decreases.

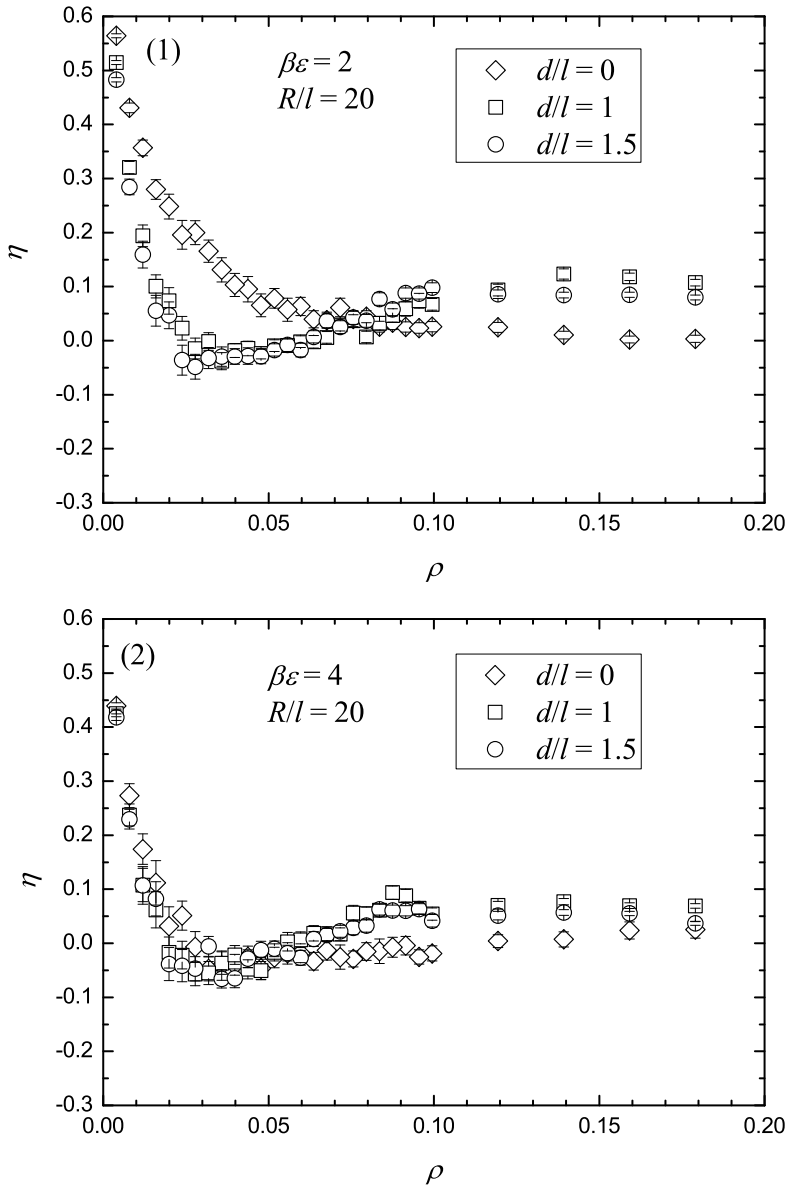

Figure 2.12: The spatial order parameter $\eta =< P_2(\cos\Theta) >$ (Eqn. 2.5) versus the surface density $\rho = N_b/4\pi R^2$ for $\beta\varepsilon = 2, 4$ and $R = 20$.

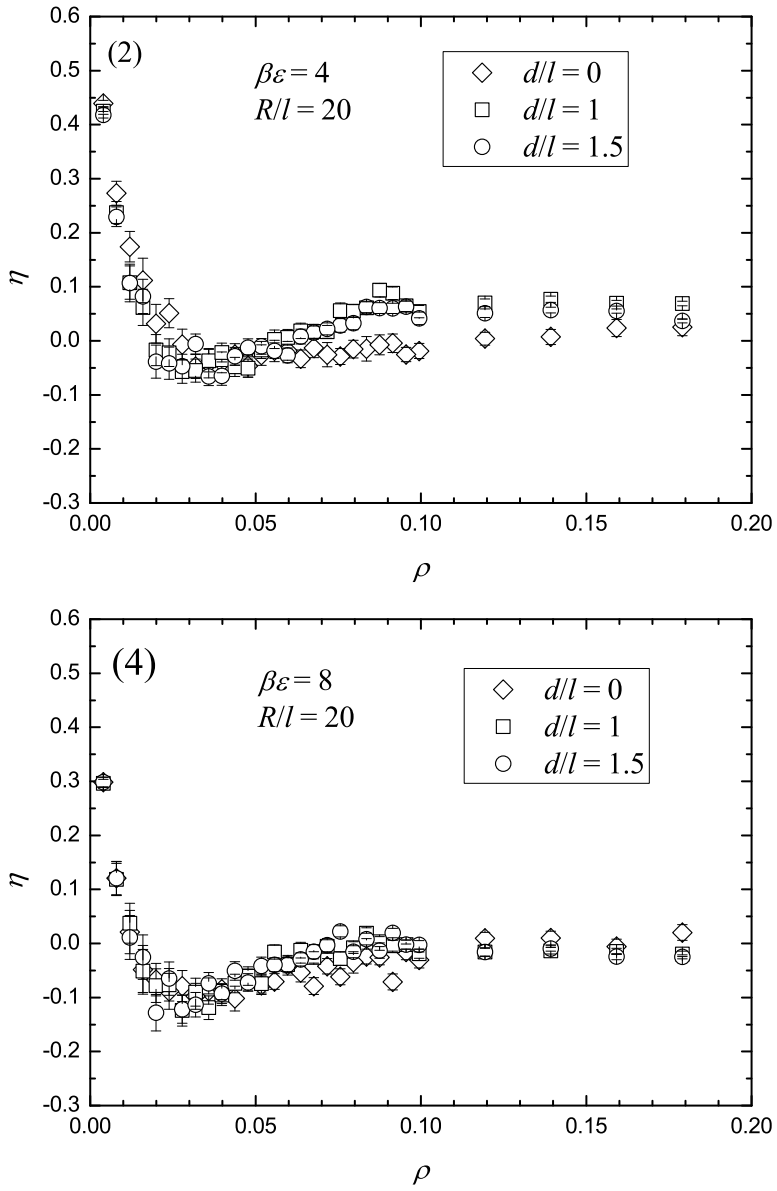

Figure 2.13: $\eta =< P_2(\cos\Theta) >$ (Eqn. 2.5) versus the surface density $\rho = N_b/4\pi R^2$ for $\beta\varepsilon = 6, 8$ and $R = 20$.

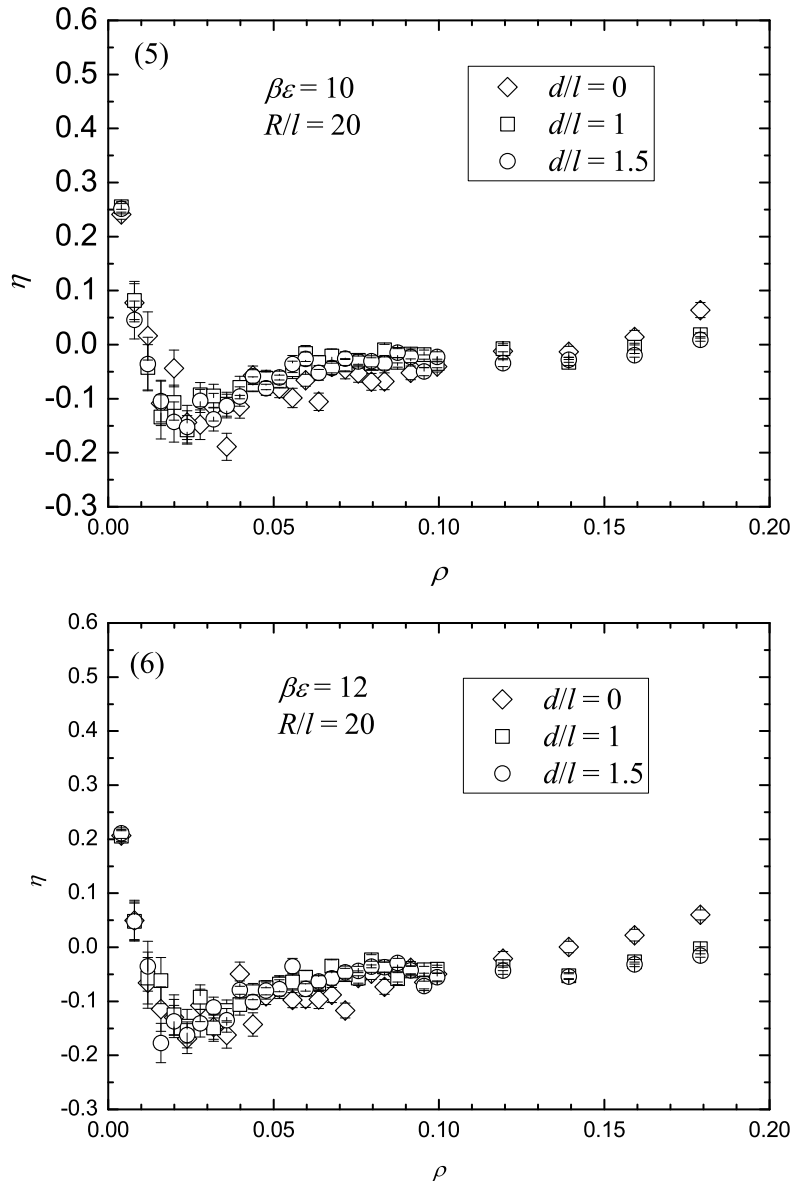

Figure 2.14: The spatial order parameter $\eta =< P_2(\cos\Theta) >$ (Eqn. 2.5) versus the surface density $\rho = N_b/4\pi R^2$ for $\beta\varepsilon = 10, 12$ and $R = 20$.

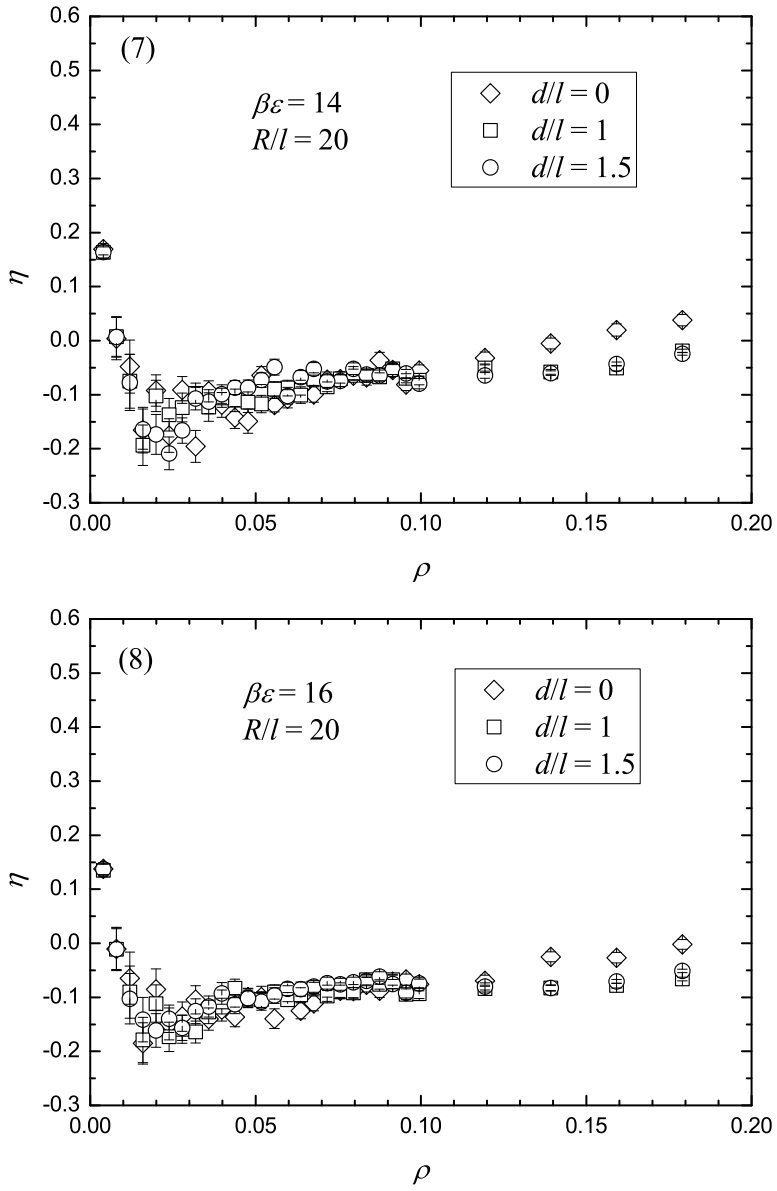

Figure 2.15: The spatial order parameter $\eta =< P_2(\cos\Theta) >$ (Eqn. 2.5) versus the surface density $\rho = N_b/4\pi R^2$ for $\beta\varepsilon = 14, 16$ and $R = 20$.

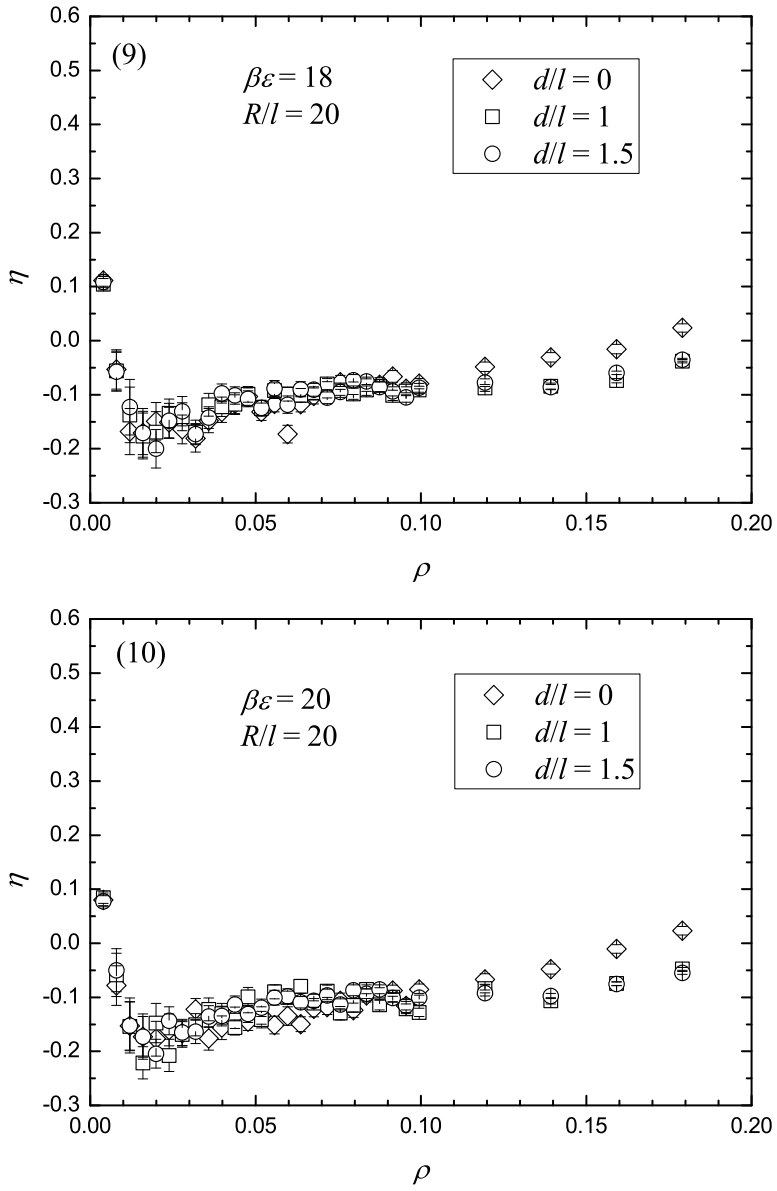

Figure 2.16: The spatial order parameter $\eta =< P_2(\cos\Theta) >$ (Eqn. 2.5) versus the surface density $\rho = N_b/4\pi R^2$ for $\beta\varepsilon = 18, 20$ and $R = 20$.

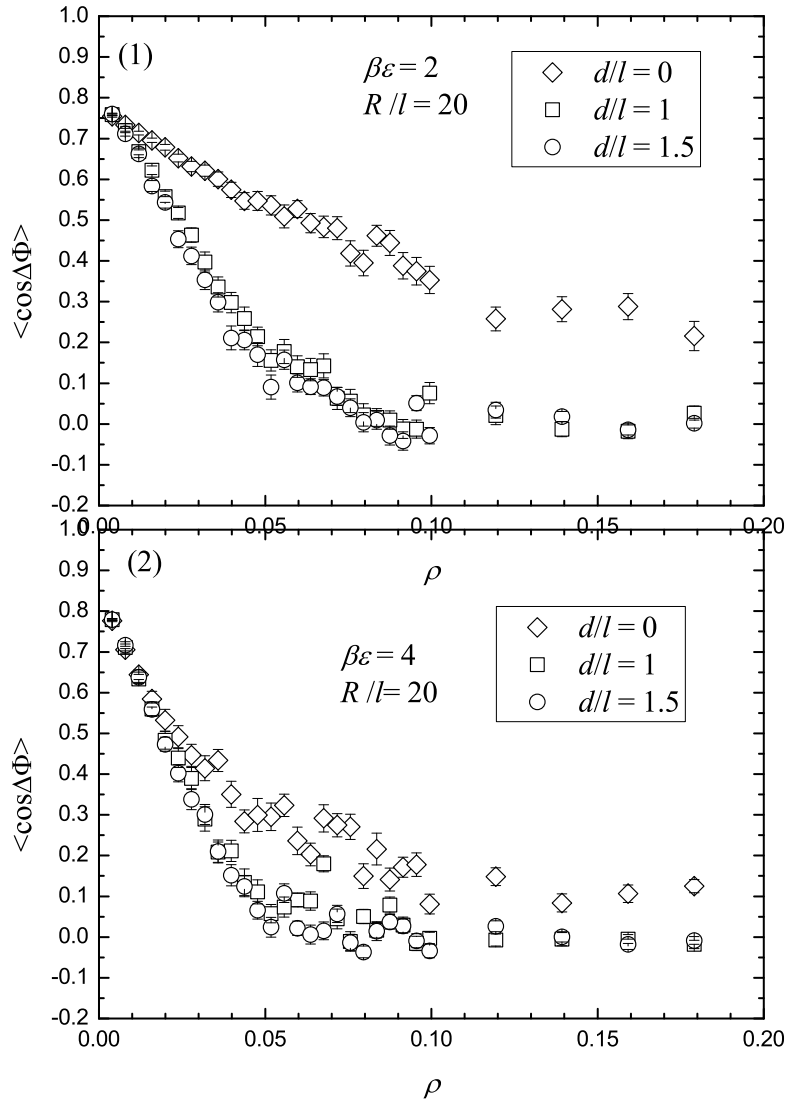

Figure 2.17: $< \cos \Delta\Phi >$ is plotted as a function of surface density ρ for $\beta\varepsilon = 2, 4$, which implies the azimuthal distribution of polymer conformation.

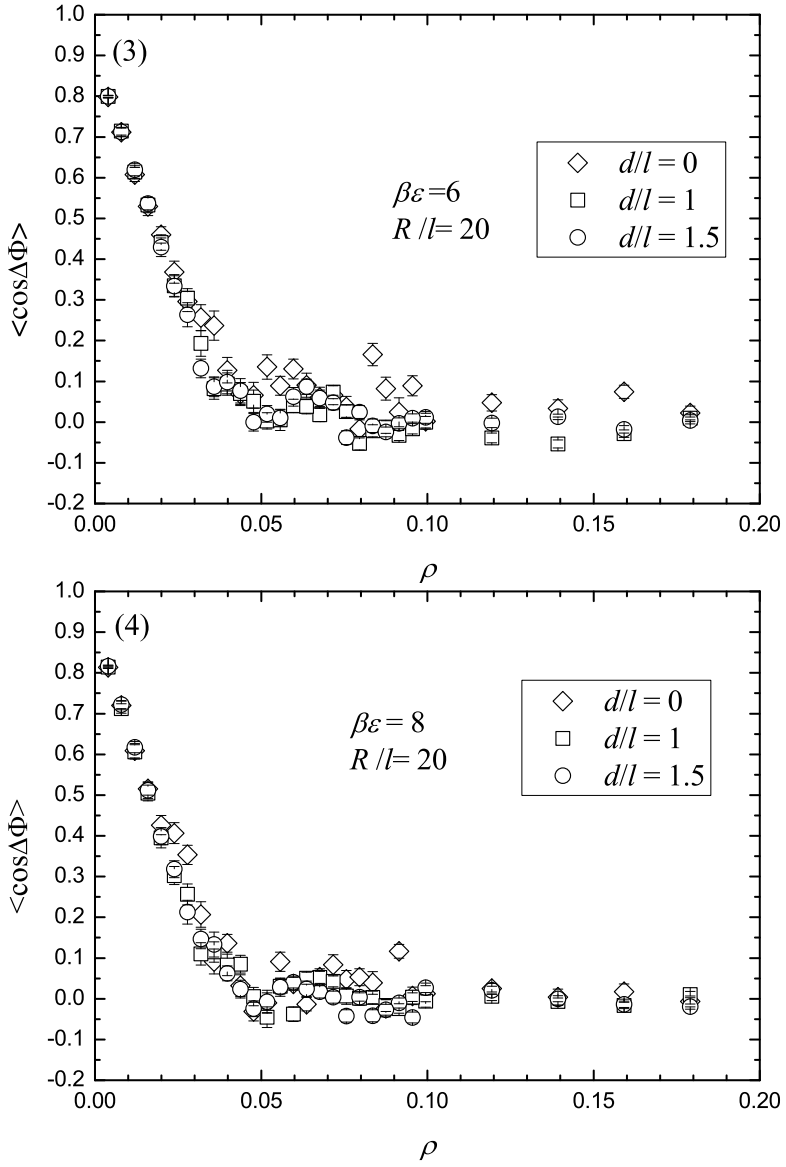

Figure 2.18: $< \cos \Delta\Phi >$ is plotted as a function of surface density ρ for $\beta\varepsilon = 6, 8$, which implies the azimuthal distribution of polymer conformation.

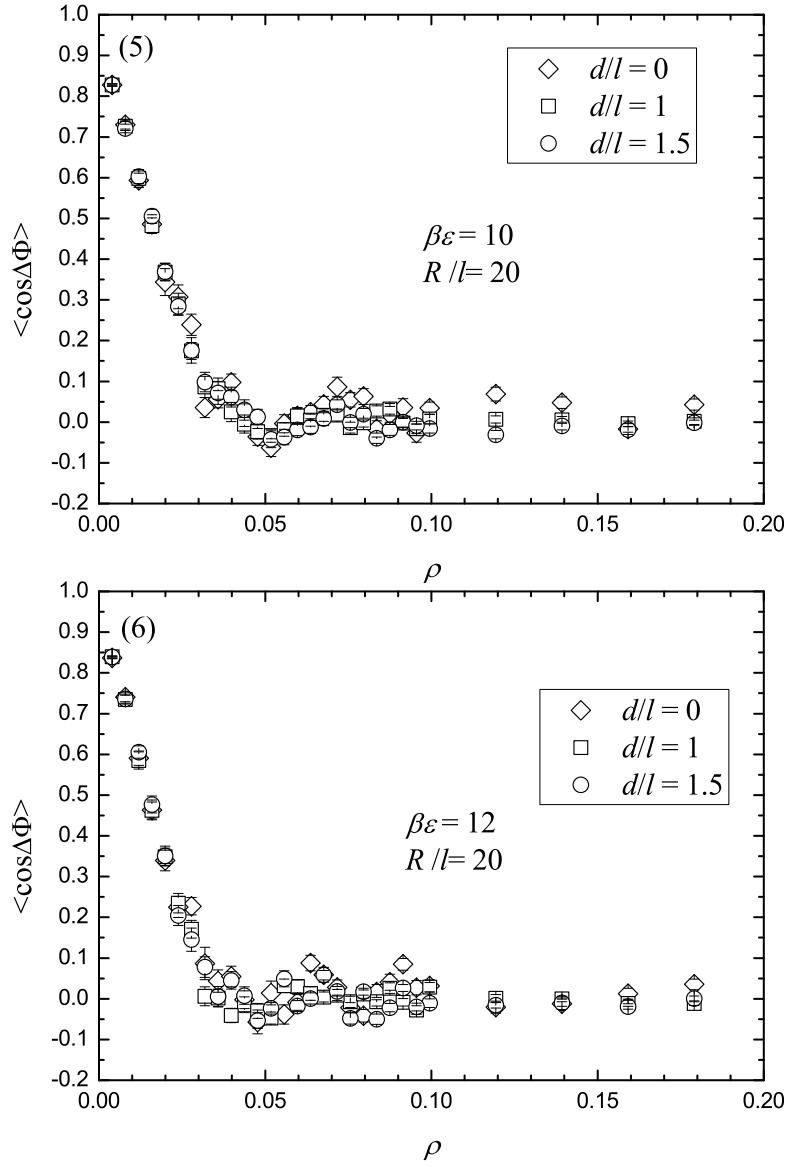

Figure 2.19: $< \cos \Delta\Phi >$ is plotted as a function of surface density ρ for $\beta\varepsilon = 10, 12$, which implies the azimuthal distribution of polymer conformation.

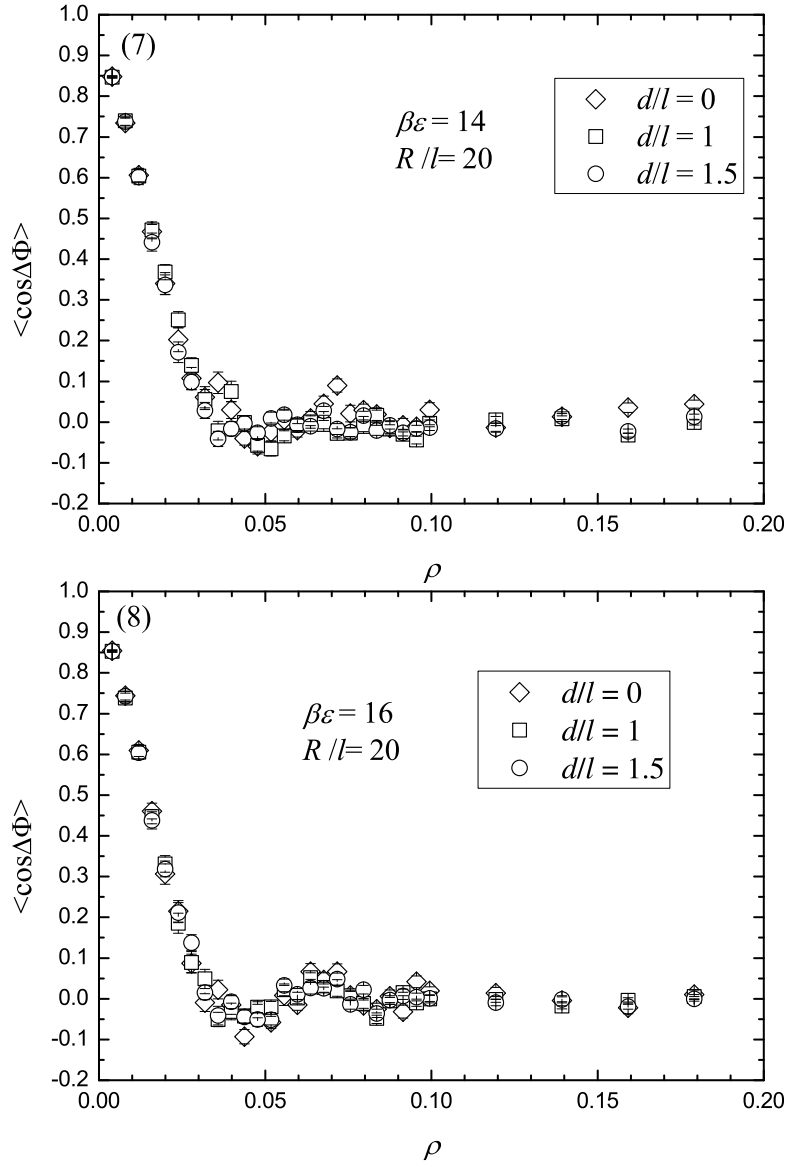

Figure 2.20: $< \cos \Delta\Phi >$ is plotted as a function of surface density ρ for $\beta\varepsilon = 14, 16$, which implies the azimuthal distribution of polymer conformation.

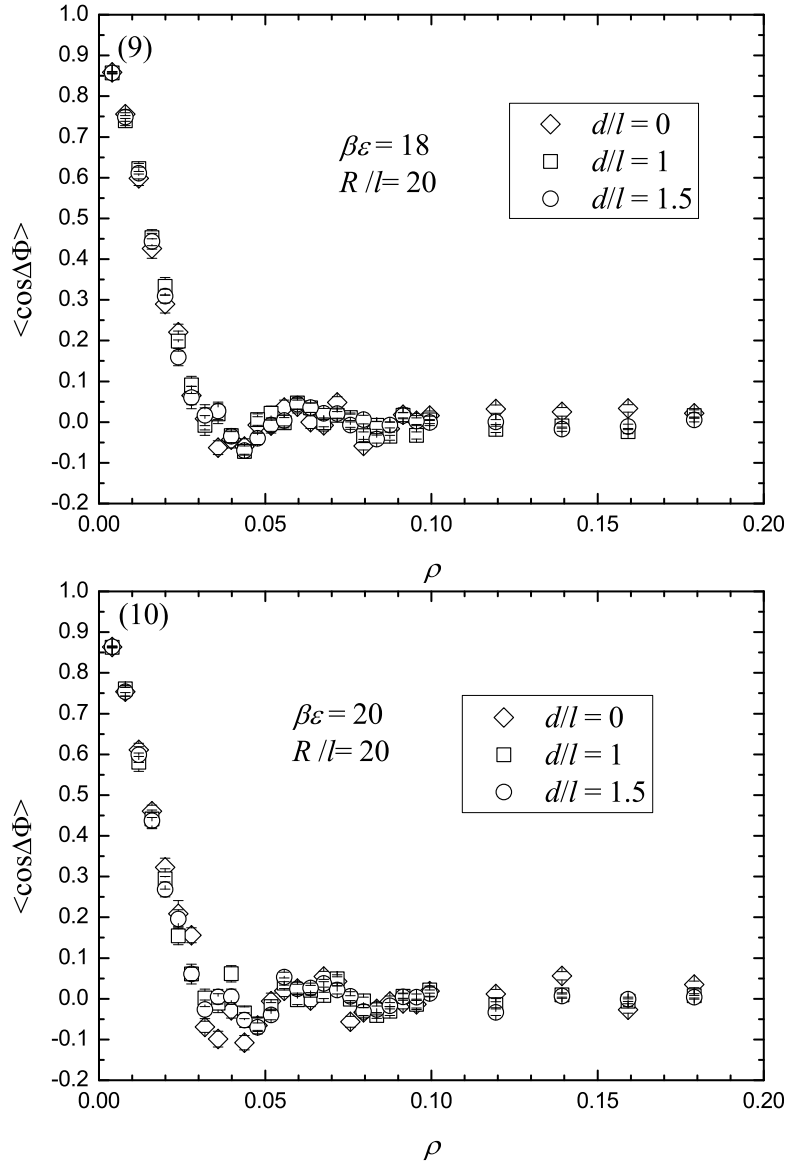

Figure 2.21: $< \cos \Delta\Phi >$ is plotted as a function of surface density ρ for $\beta\varepsilon = 18, 20$, which implies the azimuthal distribution of polymer conformation.

Chapter 3

Theoretical Analysis

3.1 Landau Expansion of Free Energy

We consider the excluded volume effect of the wormlike chain model as Onsager-like interaction. In this case the free energy per polymer chain of this system can be described by [24, 32]

$$\begin{aligned} \beta F &= -\iint \rho(\boldsymbol{r},\boldsymbol{u}) w(\boldsymbol{r},\boldsymbol{u}) d\boldsymbol{r} d\boldsymbol{u} \\ &\quad + v \iiint \rho(\boldsymbol{r},\boldsymbol{u}) \rho(\boldsymbol{r},\boldsymbol{u}') |\boldsymbol{u} \times \boldsymbol{u}'| d\boldsymbol{r} d\boldsymbol{u} d\boldsymbol{u}' \end{aligned} \tag{3.1}$$

where $\boldsymbol{r}$ is the position of polymer segment and $\boldsymbol{u}$ is the unit tangent vector of polymer segment at $\boldsymbol{r}$ (See Fig. 1.5). ρ is the segmental density distribution of polymer, which satisfies $\int \rho(\boldsymbol{r},\boldsymbol{u}) d\boldsymbol{r} d\boldsymbol{u} = N$. The total number of segments N is the ratio of the total contour length and persistence length, i.e. $N = L/l_p$. w is a mean field that is a function of $\boldsymbol{r}$ and $\boldsymbol{u}$, which would be self-consistently determined in the minimization of the free energy with respect to the density distribution. v is the excluded volume per segment. The first term determines the entropical contribution, which leads an isotropic configuration; the second term represents the excluded volume interaction that prohibits mutual penetrations of polymer chains in two-dimensional space, which prefers a parallel ordering. The isotropic-helicoidal phase transition is determined by this competition.

To express the free energy (Eqn. 3.1) in terms of ρ, it is necessary to get the relationship between the mean field w and the density distribution ρ at first, which can be derived from the diffusion-like equation (See Appendix C Eqn. C.3):

$$\left[\nabla_{\boldsymbol{u}}^2 - l_p \boldsymbol{u} \cdot \nabla_{\boldsymbol{r}}\right] q(\boldsymbol{r}, \boldsymbol{u}) = w(\boldsymbol{r}, \boldsymbol{u})\, q(\boldsymbol{r}, \boldsymbol{u}) \tag{3.2}$$

where l_p is the persistence length. The derivation of this diffusion-like equation for a semiflexible polymer chain in an external field with the idea of continuous limit of worm-like chain is quite complicated, which is described in Appendix A-C. Here the partition function $q(\boldsymbol{r}, \boldsymbol{u})$ represents the probability for a polymer chain ending at the position $\boldsymbol{r}$ and with the end vector $\boldsymbol{u}$ and it has a relationship with the density distribution ρ of polymer chain:

$$\rho(\boldsymbol{r}, \boldsymbol{u}) = q(\boldsymbol{r}, -\boldsymbol{u}) q(\boldsymbol{r}, \boldsymbol{u}) \tag{3.3}$$

because any position along the chain can be treated as two ends adjoined with opposite directions. With the definition of two angles θ and Θ (See Fig. 1.5), the integral over $\boldsymbol{r}$ and $\boldsymbol{u}$ becomes $\iint d\boldsymbol{r} d\boldsymbol{u} = 2\pi R^2 \int_0^{2\pi} \int_0^{\pi} \sin\Theta d\Theta d\theta$ and the diffusion-like equation becomes

$$\left[\frac{\partial^2}{\partial \theta^2} + \frac{l_p}{R} \sin\theta \frac{\partial}{\partial \Theta}\right] q(\Theta, \theta) = w(\Theta, \theta)\, q(\Theta, \theta) \tag{3.4}$$

With the relationship between w and ρ derived from Eqn. 3.2 and 3.3, we can express the free energy in terms of ρ. We discuss the derivation in Appendix C and show the reduced free energy here, which is divided by the total space volume $\iint d\boldsymbol{r} d\boldsymbol{u}$. The reduced free energy is expressed as a Landau expansion in terms of the averaged surface density, orientational and spatial order parameters:

$$\begin{aligned}
\tilde{F} \;=\; & 4v\bar{\varrho}^2 + \left(2 - \frac{8}{3} v\bar{\varrho}\right)\bar{\varrho}\sigma^2 + \frac{45}{512}\alpha^2\bar{\varrho}\sigma\eta + \left(\frac{225}{4096}\alpha^2 + 20v\bar{\varrho}\right)\bar{\varrho}\eta^2 \\
& - \left(\frac{2475}{3584}\alpha^2 - \frac{6075}{524288}\alpha^4\right)\bar{\varrho}\sigma\eta^2 - \frac{1125}{28672}\alpha^2\bar{\varrho}\eta^3 \\
& + \bar{\varrho}\sigma^4 + \frac{45}{1024}\alpha^2\bar{\varrho}\sigma^3\eta + \left(\frac{5}{2} - \frac{5175}{8192}\alpha^2\right)\bar{\varrho}\sigma^2\eta^2 \\
& + \left(\frac{225}{2048}\alpha^2 - \frac{30375}{1048576}\alpha^4\right)\bar{\varrho}\sigma\eta^3 \\
& + \left(\frac{30375}{401408}\alpha^2 + \frac{151875}{4194304}\alpha^4 - \frac{4100625}{4294967296}\alpha^6\right)\bar{\varrho}\eta^4 + \mathscr{O}\left(\sigma^5\right)
\end{aligned} \tag{3.5}$$

where $\bar{\varrho}$ is associated with the averaged surface density $\varrho = N/4\pi R^2$ in the relationship $\bar{\varrho} = \varrho/2\pi$. The order parameters σ and η represent the orientational and spatial distribution of the polymer chain respectively, which are defined as $\sigma =< \cos 2\theta >$ and $\eta =< P_2(\cos\Theta) >$ (See Eqn. 1.5 and 1.6). And $\alpha = \pi l_p/R$, where l_p is the persistence length of the polymer chain and R is the radius of the spherical surface.

Then we define $n = v\varrho = 2\pi v\bar{\varrho} = Nl_p^2/4\pi R^2$, which is the ratio of total excluded volume and total space volume as defined in Chapter 2 (Eqn. 2.9). Then the free energy can be rewritten as:

$$\begin{aligned}
\tilde{F} \;=\; & \bar{\varrho}\left[4\bar{n} + \left(2 - \frac{8}{3}\bar{n}\right)\sigma^2 + \frac{45}{512}\alpha^2\sigma\eta + \left(\frac{225}{4096}\alpha^2 + 20\bar{n}\right)\eta^2\right. \\
& -\left(\frac{2475}{3584}\alpha^2 - \frac{6075}{524288}\alpha^4\right)\sigma\eta^2 - \frac{1125}{28672}\alpha^2\eta^3 \\
& +\sigma^4 + \frac{45}{1024}\alpha^2\sigma^3\eta + \left(\frac{5}{2} - \frac{5175}{8192}\alpha^2\right)\sigma^2\eta^2 \\
& +\left(\frac{225}{2048}\alpha^2 - \frac{30375}{1048576}\alpha^4\right)\sigma\eta^3 \\
& \left.+\left(\frac{30375}{401408}\alpha^2 + \frac{151875}{4194304}\alpha^4 - \frac{4100625}{4294967296}\alpha^6\right)\eta^4 + \mathcal{O}\left(\sigma^5\right)\right] \qquad (3.6)
\end{aligned}$$

where $\bar{n} = v\bar{\varrho} = n/2\pi$ for convenience. The expression in the square bracket above as a function of order parameters σ and η depends on the two dimensionless parameters n and α. This means, for any given α, the value of n determines the equilibrium conformation of polymer chain by minimizing the free energy with respect to both orientational and spatial order parameters.

3.2 Order Parameters of Wormlike Chains

The minimization conditions for the free energy of two order parameters (Eqn. 3.6) can be written as $\partial\tilde{F}/\partial\sigma = \partial\tilde{F}/\partial\eta = 0$, $\partial^2\tilde{F}/\partial\sigma^2 > 0$ and $\partial^2\tilde{F}/\partial\eta^2 > 0$. First, we take the limit $\alpha = \pi l_p/R \to 0$. It eliminates all of the coupling terms, including both σ and η, and cubic terms so as to automatically set the spatial distribution parameter η be zero in the minimization of free energy. Then the free energy describes a polymer chain confined

to a plane, where only the square and quartic terms of σ survive. This implies a second order isotropic-nematic phase transition [6].

Second, we reduce the expansion of free energy to one-parameter to solve the minimization analytically. Because of the positive coefficient for the square term η^2, the minimization condition $\partial^2\tilde{F}/\partial\eta^2 > 0$ can be always satisfied near the critical point. We can determine the expression of η in terms of σ by setting the first order differential of the free energy be zero, i.e. $\partial\tilde{F}/\partial\eta = 0$ and write it as an expansion:

$$\eta = b_1\sigma + b_2\sigma^2 + b_3\sigma^3 \tag{3.7}$$

where

$$b_1 = -\frac{45}{512}\alpha^2 \Big/ \left(\frac{225}{2048}\alpha^2 + 40n\right) \tag{3.8}$$

$$b_2 = \left(\frac{2475}{1792}\alpha^2 b_1 - \frac{6075}{262144}\alpha^4 b_1 + \frac{3375}{28672}\alpha^2 b_1^2\right) \Big/ \left(\frac{225}{2048}\alpha^2 + 40\bar{n}\right) \tag{3.9}$$

$$\begin{aligned} b_3 = &-\left(\frac{45}{1024}\alpha^2 + 5b_1 - \frac{5175}{4096}\alpha^2 b_1 + \frac{675}{2048}\alpha^2 b_1^2 - \frac{91125}{1048576}\alpha^4 b_1^2\right. \\ &+\frac{30375}{100352}\alpha^2 b_1^3 + \frac{151875}{1048576}\alpha^4 b_1^3 - \frac{4100625}{1073741824}\alpha^6 b_1^3 - \frac{3375}{14336}\alpha^2 b_1 b_2 \\ &\left.-\frac{2475}{1792}\alpha^2 b_2 + \frac{6075}{262144}\alpha^4 b_2\right) \Big/ \left(\frac{225}{2048}\alpha^2 + 40\bar{n}\right) \end{aligned} \tag{3.10}$$

The coefficient b_1 in front of the leading term in Eqn. 3.7 is always negative, which is the dominant reason for the physical situation that η has an opposite sign to σ. In other words, for positive σ, which implies the polymer has higher probability to appear parallel to the equator of the spherical surface, η would be negative, which means the higher probability near the equator (Fig. 1.6.b).

Then, with Eqn. 3.7, the spatial order parameter η can be replaced by the orientational one σ in the expression of the reduced free energy (Eqn. 3.6), which becomes

$$\tilde{F} = \bar{\varrho}\left[4\bar{n} + c_2\sigma^2 + c_3\sigma^3 + c_4\sigma^4 + \mathscr{O}\left(\sigma^5\right)\right] \tag{3.11}$$

where

$$c_2 = 2 - \frac{8}{3}\bar{n} + \frac{45}{512}\alpha^2 b_1 + \frac{225}{4096}\alpha^2 b_1^2 + 20\bar{n}b_1^2 \tag{3.12}$$

$$c_3 = -\frac{2475}{3584}\alpha^2 b_1^2 + \frac{6075}{524288}\alpha^4 b_1^2 - \frac{1125}{28672}\alpha^2 b_1^3 + \frac{45}{512}\alpha^2 b_2 + \frac{225}{2048}\alpha^2 b_1 b_2 + 40\bar{n}b_1 b_2 \tag{3.13}$$

$$\begin{aligned} c_4 = {} & 1 + \frac{5}{2}b_1^2 + \frac{45}{1024}\alpha^2 b_1 + \frac{5175}{8192}\alpha^2 b_1^2 + \frac{225}{2048}\alpha^2 b_1^3 - \frac{2475}{1792}\alpha^2 b_1 b_2 \\ & - \frac{3375}{28672}\alpha^2 b_1^2 b_2 + \frac{45}{512}\alpha^2 b_3 + \frac{225}{2048}\alpha^2 b_1 b_3 + \frac{30375}{401408}\alpha^2 b_1^4 \\ & + \frac{151875}{4194304}\alpha^4 b_1^4 - \frac{4100625}{4294967296}\alpha^6 b_1^4 + \frac{225}{4096}\alpha^2 b_2^2 \\ & + 40\bar{n}b_1 b_3 + 20\bar{n}b_2^2 \end{aligned} \tag{3.14}$$

Here the coefficients c_2, c_3 and c_4 are the functions of n and α.

For any given n and α, the orientational order parameter corresponding to the equilibrium configuration of the polymer chain can be obtained by minimizing the single-order-parameter free energy (Eqn. 3.11) with respect to the orientational order parameter σ. The minimization conditions are $\partial\tilde{F}/\partial\sigma = 0$ and $\partial^2\tilde{F}/\partial\sigma^2 > 0$. The spatial order parameter can be regained by Eqn. 3.7. The stable configuration of the polymer chain confined to a spherical surface is determined by n, the ratio of total excluded volume and total space volume, and α, the ratio of the persistence length and the sphere radius. Therefore, for a given l_p/R, we can obtain the critical value of n according to the minimization of free energy. For $0 < l_p/R \leq 2$, the coefficient c_4 keeps positive, which is responsible for stabilizing the system, and c_3 in front of the cubic term is negative, which warrants that the isotropic-helicoidal phase transition is first order and the orientational order parameter σ is positive at the helicoidal phase. The critical value of n is mainly determined by the leading term $2 - 8\bar{n}/3$ in the expression of c_2, which is positive for low density and becomes negative for higher.

By minimizing the free energy, two phases can be detected. Fig. 3.1 and Fig. 3.2 show the free energy and order parameters versus n for $l_p/R = 1$ and $l_p/R = 2$. Both the orientational and spatial order parameters eliminate in disordered phase at low surface density. At a sufficiently high density, the free energy bifurcates. The lower one corresponds to the helicoidal phase with non-zero order parameters. The positive orientational

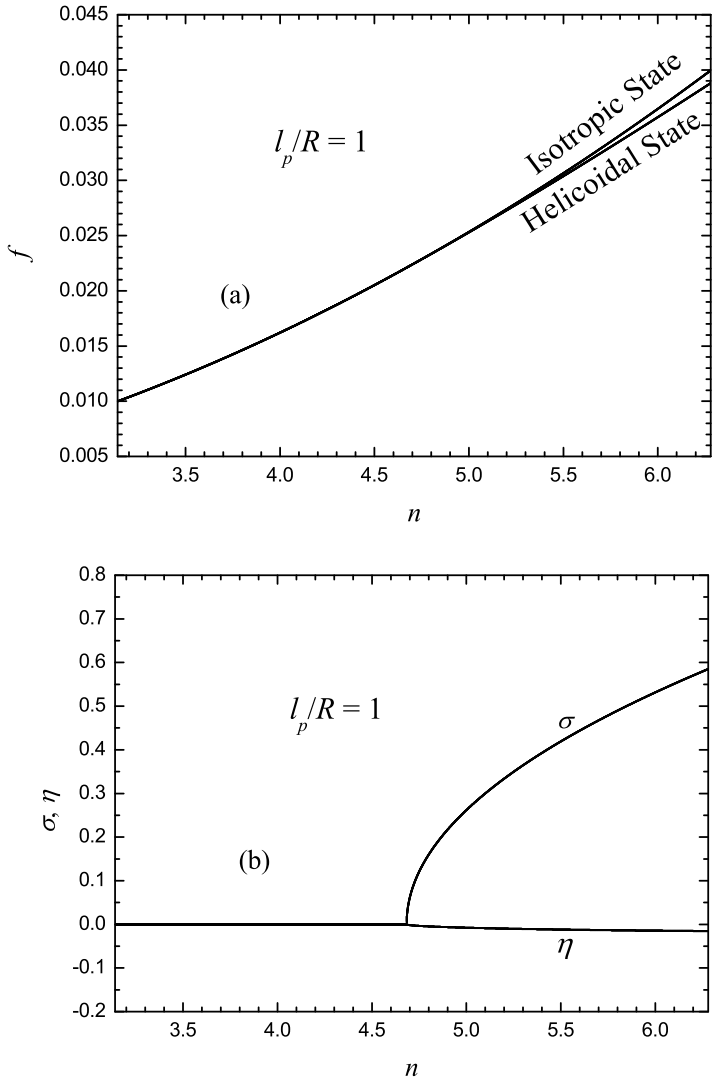

Figure 3.1: (a) The free energy $f = \tilde{F} = \beta F/8\pi^2 R^2$ and (b) the orientational order parameter $\sigma =< \cos\theta >$ and spatial order parameter $\eta =< P_2(\cos\Theta) >$ versus $n = Nl_p^2/4\pi R^2$ for $l_p/R = 1$

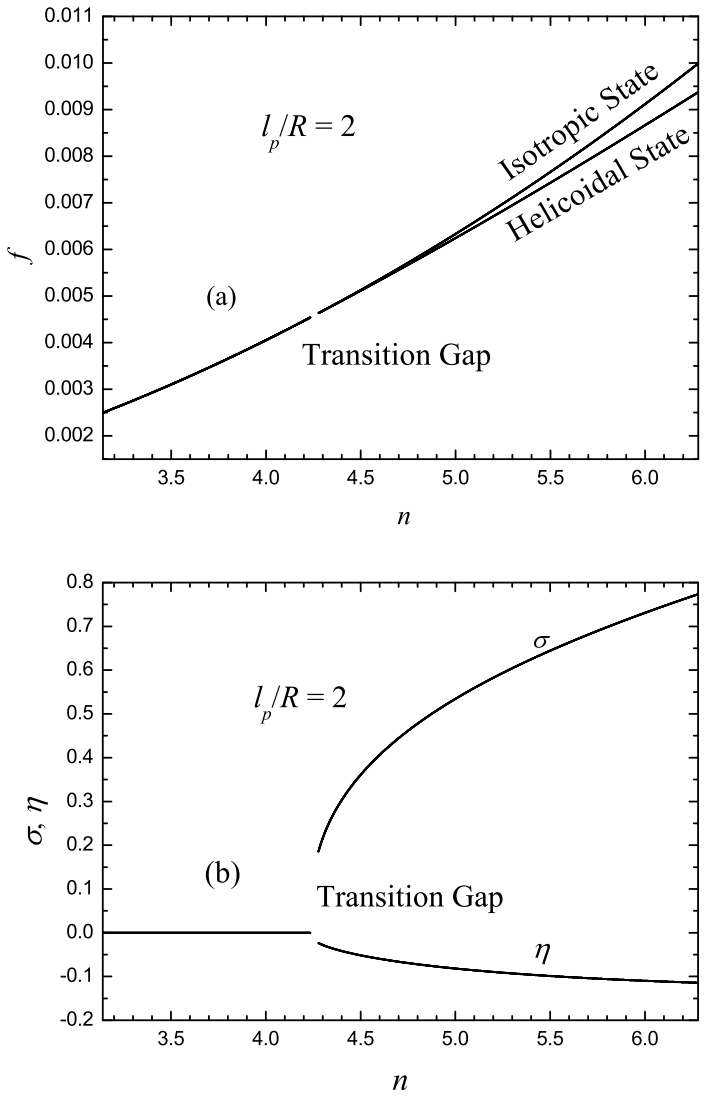

Figure 3.2: (a) The free energy $f = \tilde{F} = \beta F/8\pi^2 R^2$ and (b) the orientational order parameter $\sigma =< \cos\theta >$ and spatial order parameter $\eta =< P_2(\cos\Theta) >$ versus $n = Nl_p^2/4\pi R^2$ for $l_p/R = 2$

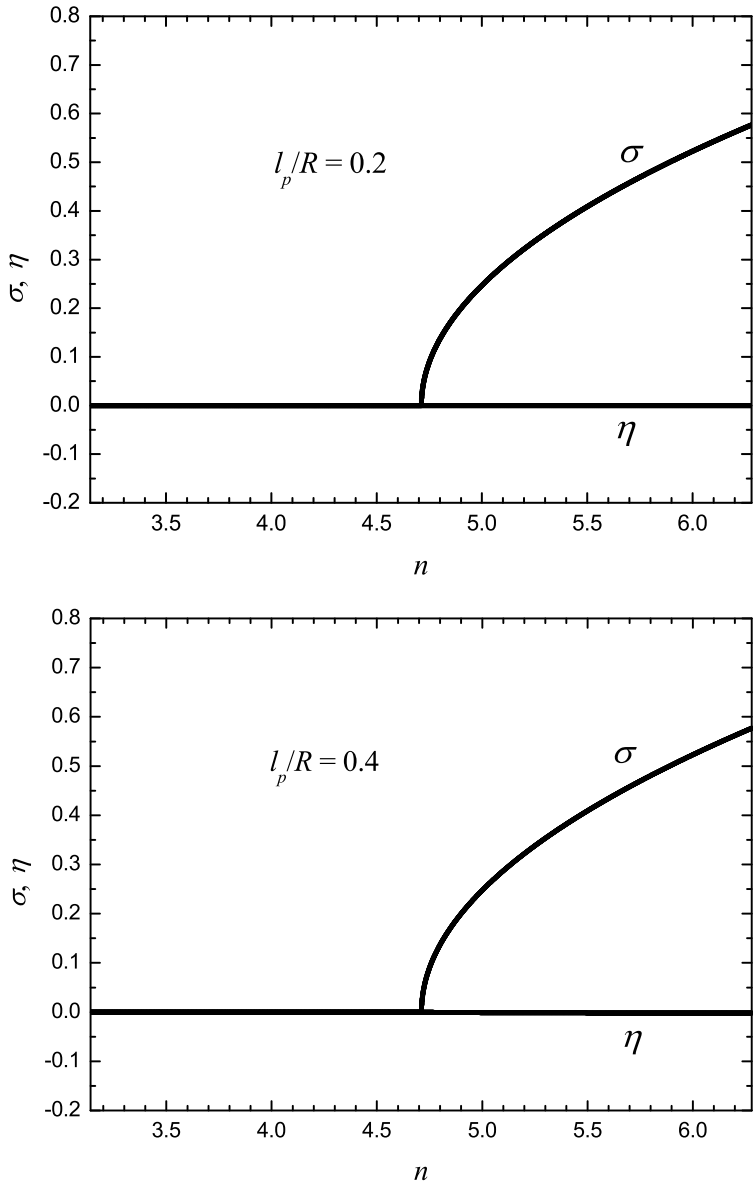

Figure 3.3: The order parameters σ and η versus $n = Nl_p^2/4\pi R^2$ for $l_p/R = 0.2, 0.4$.

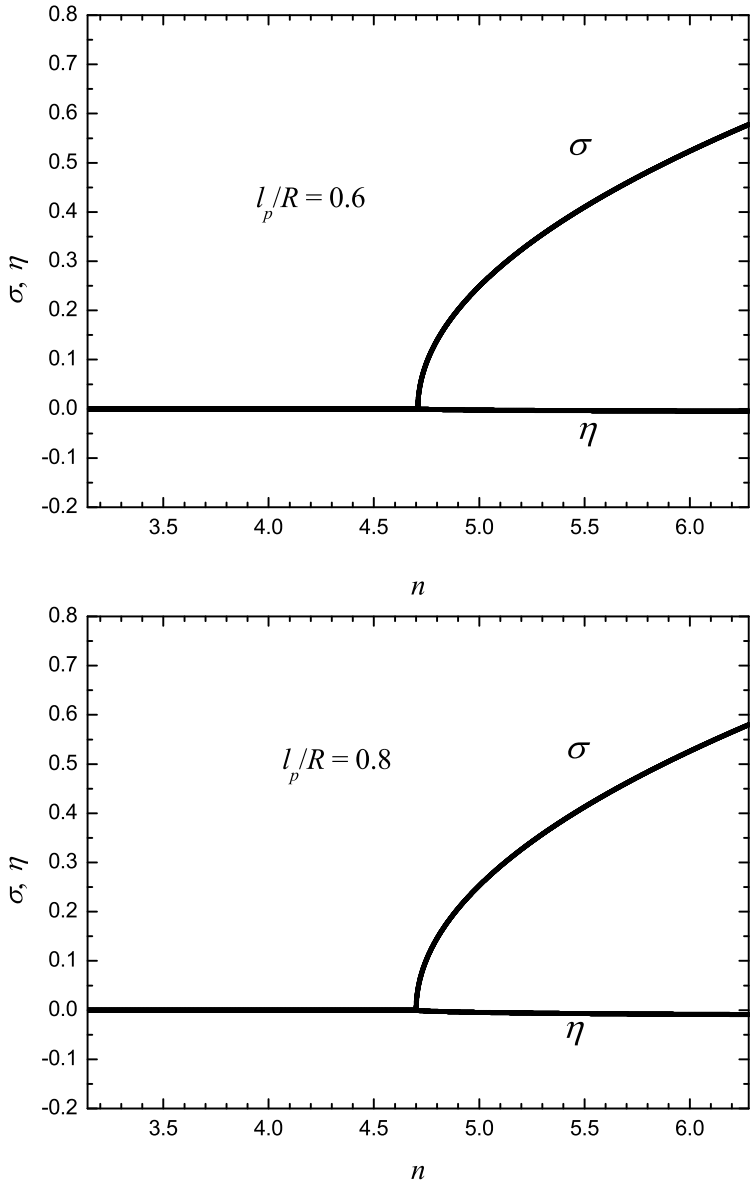

Figure 3.4: The order parameters σ and η versus $n = Nl_p^2/4\pi R^2$ for $l_p/R = 0.6, 0.8$.

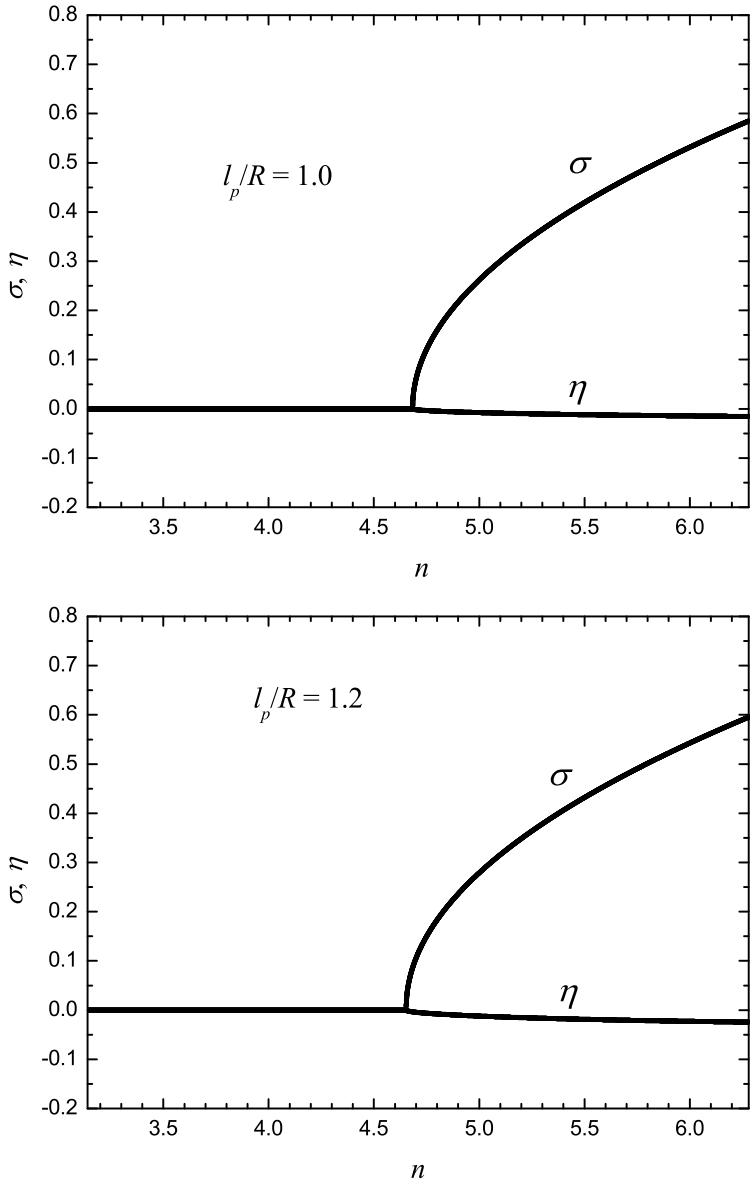

Figure 3.5: The order parameters σ and η versus $n = Nl_p^2/4\pi R^2$ for $l_p/R = 1.0, 1.2$.

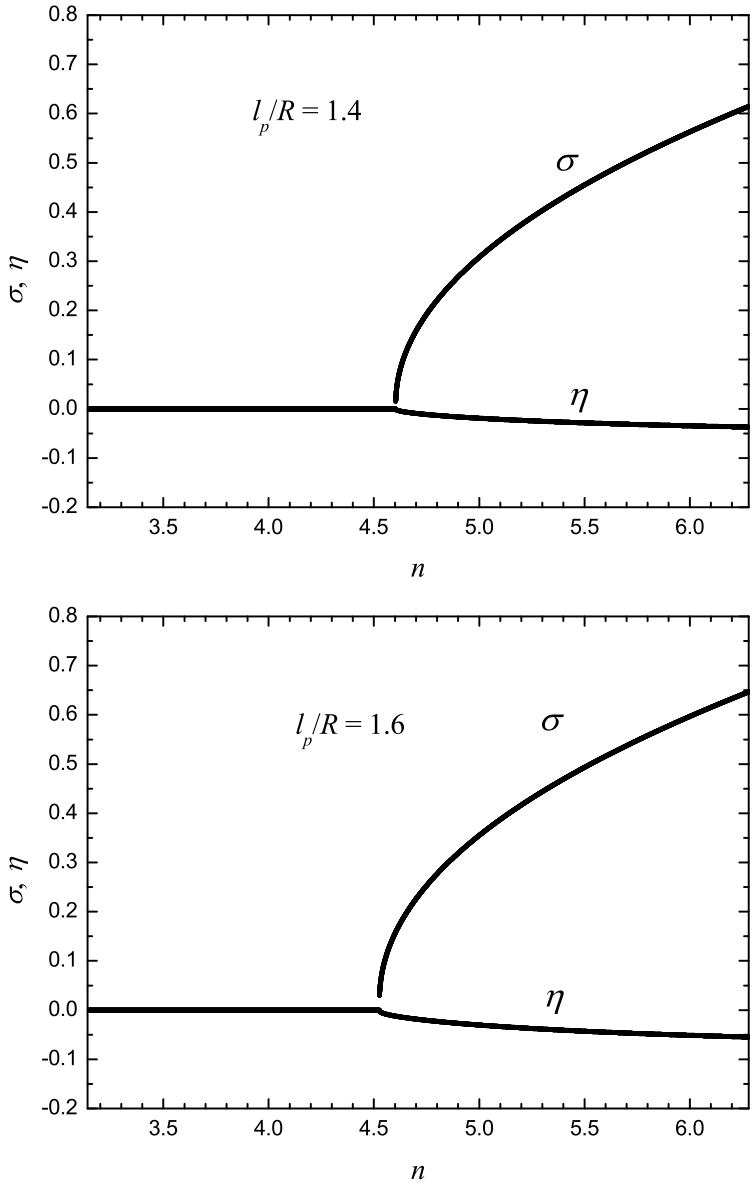

Figure 3.6: The order parameters σ and η versus $n = Nl_p^2/4\pi R^2$ for $l_p/R = 1.4, 1.6$.

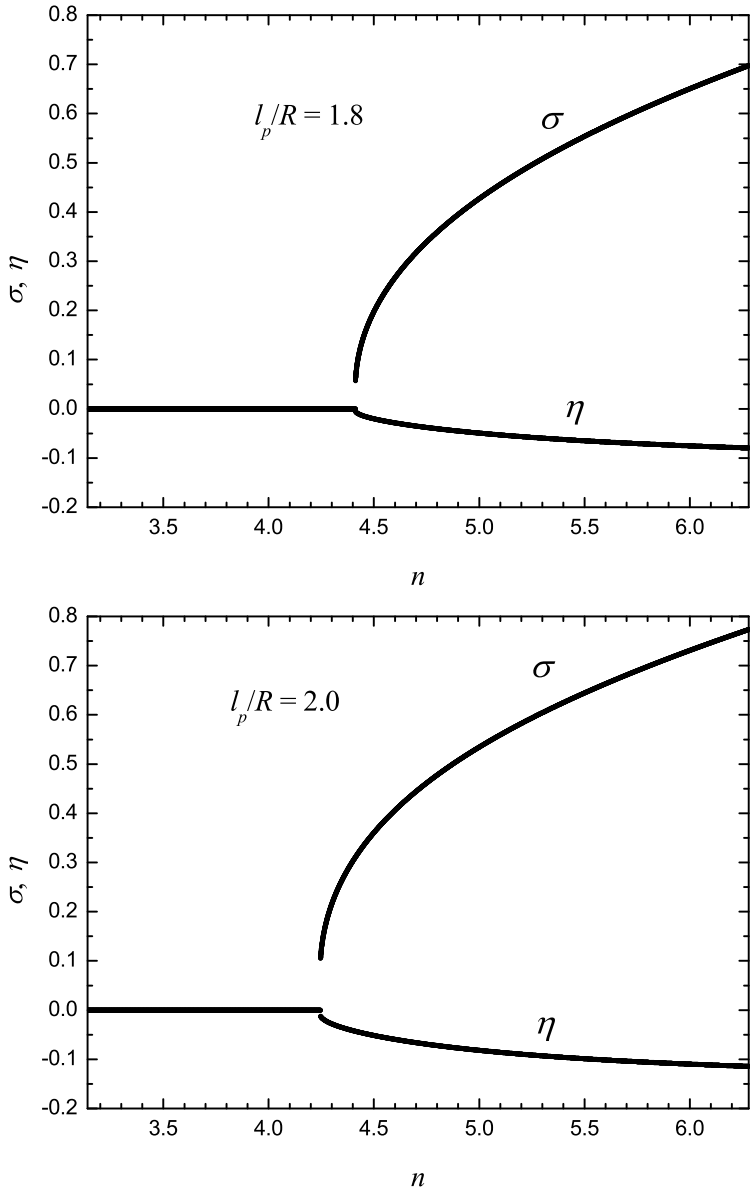

Figure 3.7: The order parameters σ and η versus $n = Nl_p^2/4\pi R^2$ for $l_p/R = 1.8, 2.0$.

order parameter σ indicates that the polymer chain has more probability to be parallel to the equator so as to form a helicoidal conformation (See Fig. 1.6.b). The negative spatial order parameter η illuminates that the polymer chain at helicoidal state tends to occupy the positions near the equator in order to hold low bending energy because of the less curvature near the equator, which has been verified by the computer simulations.

By comparing Fig. 3.2 with Fig. 3.1 and even more cases (See Fig. 3.3-3.7), we can notice that for greater l_p/R the phase transition occurs at lower density, because the excluded volume effect becomes stronger for longer persistence length on the spherical surface and the polymer segments have greater tendency to be parallel to each other. By comparing Fig. 3.3-3.7 with Fig. 2.6-2.10 in Chapter 2, we show the orientational order parameters at various density for $l_p/R = 1$ and $l_p/R = 2$ from both simulation and theoretical analysis in Fig. 3.8.a and 3.9.a, respectively. The order parameters are plotted as a function of n/n_c to move the curves to the same reference point, i.e. critical point, in Fig. 3.8.b and 3.9.b. We can notice that the theoretical analysis also shows the existence of the helicoidal state at high density, which is reasonably similar as the result from computer simulation. But the critical values of n are different, which will be discussed in next section.

3.3 Isotropic-Helicoidal Phase Transition

To obtain the transition gap of the first-order isotropic-helicoidal phase transition, the minimized free energy should be rewritten as the function of the averaged surface density $\bar{\varrho}$ for both of two phases. For the isotropic phase, the free energy would be $\tilde{F}_{iso} = 4v\bar{\varrho}_{iso}^2$, and for the helicoidal phase, $\tilde{F}_{hel} = f_1\bar{\varrho}_{hel} + f_2\bar{\varrho}_{hel}^2$, where f_1 and f_2 are the functions of n,

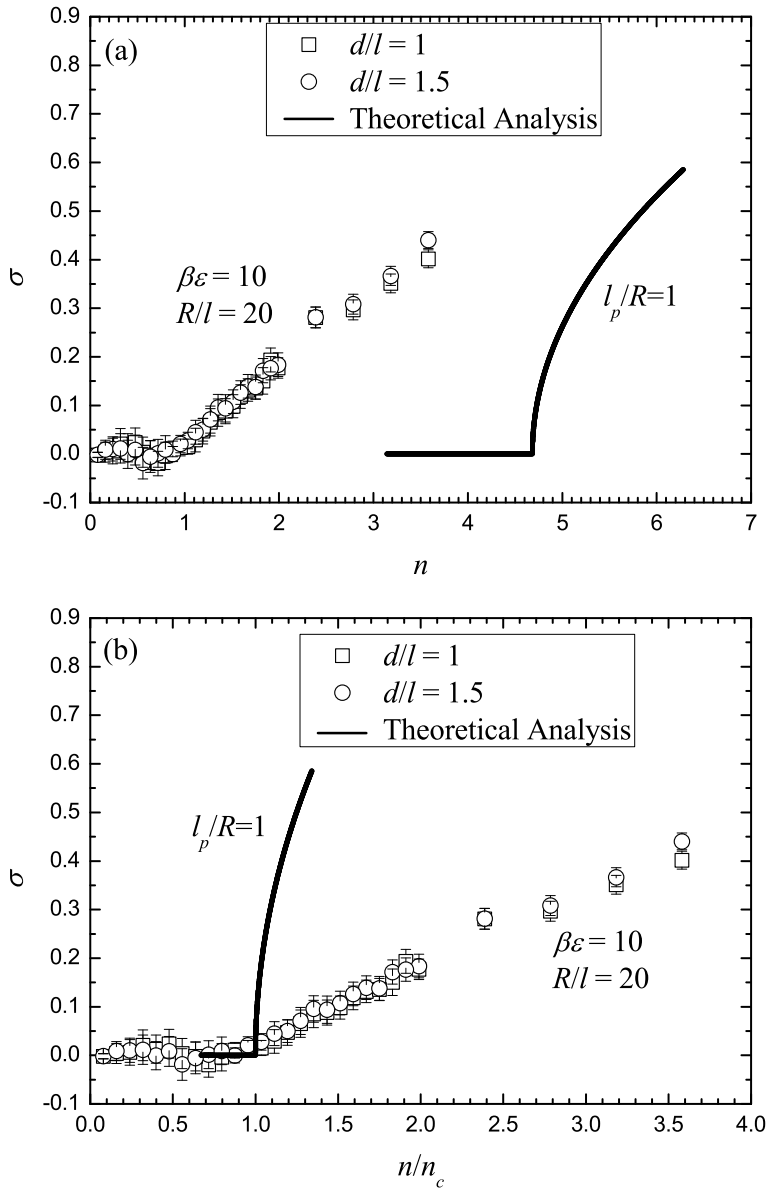

Figure 3.8: The orientational order parameter σ versus $n = Nl_p^2/4\pi R^2$ for $l_p/R = 1$.

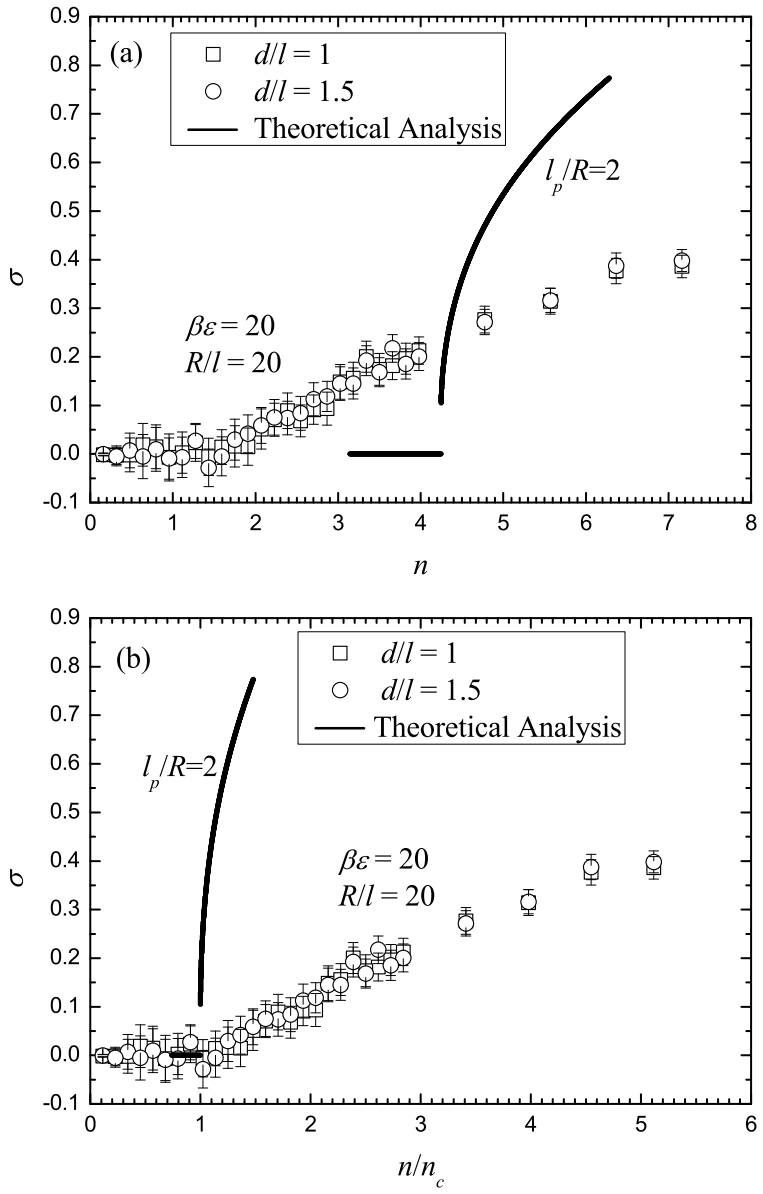

Figure 3.9: The orientational order parameter σ versus $n = Nl_p^2/4\pi R^2$ for $l_p/R = 2$.

α, σ, and η:

$$
\begin{aligned}
f_1 &= 2\sigma^2 + \frac{45}{512}\alpha^2\sigma\eta + \frac{225}{4096}\alpha^2\eta^2 \\
&\quad -\left(\frac{2475}{3584}\alpha^2 - \frac{6075}{524288}\alpha^4\right)\sigma\eta^2 - \frac{1125}{28672}\alpha^2\eta^3 \\
&\quad +\sigma^4 + \frac{45}{1024}\alpha^2\sigma^3\eta + \left(\frac{5}{2} - \frac{5175}{8192}\alpha^2\right)\sigma^2\eta^2 \\
&\quad +\left(\frac{225}{2048}\alpha^2 - \frac{30375}{1048576}\alpha^4\right)\sigma\eta^3 \\
&\quad +\left(\frac{30375}{401408}\alpha^2 + \frac{151875}{4194304}\alpha^4 - \frac{4100625}{4294967296}\alpha^6\right)\eta^4 \qquad (3.15) \\
f_2 &= v\left(4 - \frac{8}{3}\sigma^2 + 20\eta^2\right) \qquad (3.16)
\end{aligned}
$$

Here the order parameters σ and η correspond to the stable configuration.

For phase equilibrium, the chemical potential and pressure should be equal to each other in both of two phases [17]:

$$
\begin{aligned}
\mu_{iso}\left(\bar{\varrho}_{iso}\right) &= \mu_{hel}\left(\bar{\varrho}_{hel}\right) \qquad (3.17) \\
\Pi_{iso}\left(\bar{\varrho}_{iso}\right) &= \Pi_{hel}\left(\bar{\varrho}_{hel}\right) \qquad (3.18)
\end{aligned}
$$

The chemical potential and pressure can be obtained from the free energy: $\mu = \partial\tilde{F}/\partial\bar{\varrho}$ and $\Pi = \mu\bar{\varrho} - \tilde{F}$, respectively. For various value of α, i.e. l_p/R, the equilibrium densities $\bar{\varrho}_{hel}$ and $\bar{\varrho}_{iso}$ can be determined by solving the equations 3.17 and 3.18. The transition gap is defined by $\Delta\bar{\varrho} = \bar{\varrho}_{hel} - \bar{\varrho}_{iso}$.

The expressions of f_1 and f_2 contain both order parameters σ and η, which must be determined by minimizing the free energy at first. Therefore, f_1 and f_2 in the expression of $\tilde{F}_{hel}$ are actually the implicit functions of ϱ. Then we would like to both analytically and numerically solve the phase equilibrium equations (Eqn. 3.17 and 3.18) incorporated with the minimization of free energy. To obtain the analytical solution, we have to consider more approximations to simplify and expand the expressions of f_1 and f_2 in terms of $\alpha/10$, where we set $0 < l_p/R \leq 2$ so $|\alpha/10| < 1$. The analytical solutions of

equilibrium densities and transition gap can be described as expansions in terms of $\alpha/10$:

$$\begin{aligned}
\bar{\varrho}_{hel} &= \frac{f_1}{4\sqrt{vf_2} - 2f_2} \\
&= \frac{1}{v}\left[\frac{3}{4} + A_4\left(\frac{\alpha}{10}\right)^4 + A_6\left(\frac{\alpha}{10}\right)^6 + A_8\left(\frac{\alpha}{10}\right)^8\right. \\
&\quad \left. + A_{10}\left(\frac{\alpha}{10}\right)^{10} + A_{12}\left(\frac{\alpha}{10}\right)^{12} + A_{14}\left(\frac{\alpha}{10}\right)^{14} + \mathscr{O}\left(\left(\frac{\alpha}{10}\right)^{16}\right)\right] \qquad (3.19) \\
\bar{\varrho}_{iso} &= \sqrt{\frac{f_2}{4v}}\bar{\varrho}_{hel} \\
&= \frac{1}{v}\left[\frac{3}{4} + A_4\left(\frac{\alpha}{10}\right)^4 + A_6\left(\frac{\alpha}{10}\right)^6 + A_8\left(\frac{\alpha}{10}\right)^8\right. \\
&\quad \left. + A_{10}\left(\frac{\alpha}{10}\right)^{10} + B_{12}\left(\frac{\alpha}{10}\right)^{12} + B_{14}\left(\frac{\alpha}{10}\right)^{14} + \mathscr{O}\left(\left(\frac{\alpha}{10}\right)^{16}\right)\right] \qquad (3.20) \\
\Delta\bar{\varrho} &= \bar{\varrho}_{hel} - \bar{\varrho}_{iso} \\
&= \frac{1}{v}\left[C_{12}\left(\frac{\alpha}{10}\right)^{12} + C_{14}\left(\frac{\alpha}{10}\right)^{14} + \mathscr{O}\left(\left(\frac{\alpha}{10}\right)^{16}\right)\right] \qquad (3.21)
\end{aligned}$$

where $A_4 \approx -0.483$, $A_6 \approx 1.5 \times 10^{-10}$, $A_8 \approx -0.686$, $A_{10} \approx 0.683$, $A_{12} \approx -0.083$, $A_{14} \approx -0.031$, $B_{12} \approx -5.023$, $B_{14} \approx 7.206$, $C_{12} \approx 4.940$, and $C_{14} \approx -7.237$.

Fig. 3.10 shows the equilibrium densities and transition gap for $0 < l_p/R \leq 2$ from both analytical and numerical methods. They are in reasonable agreement with each other, which verifies that the analytical solutions (Eqn. 3.19-3.21) give reasonable results. The constant term $3/4v$ in the expansions of the equilibrium surface densities for both of the isotropic and helicoidal phases comes from the coefficient of the square term σ^2 in the free energy (Eqn. 3.11), which represents the general phase transition property of polymer chains in two dimensions. For a polymer chain with $L >> l_p$, where L is the total contour length, the critical density of the isotropic-nematic phase transition is constant [6]. The second term of the equilibrium densities, i.e. the first-rank correction, which is proportional to α^4, comes from the spatial distribution, whose leading term is proportional to $\alpha^2\sigma$. This term dominates the decrease of critical value of n for large l_p/R in Fig. 3.10. The width of transition gap $\Delta\bar{\varrho}$ comes from the coefficients in front of the cubic terms in Eqn. 3.11. In other words, if the cubic term didn't exist, the system would exhibit a continuous phase transition without any transition gap. In addition, the width of transition gap, whose leading term is of order $(\alpha/10)^{12}$, is quite small relative to the

critical density with the leading term 3/4. Therefore, the isotropic-helicoidal transition is a "weak" first order one. This could also explain that we didn't detect an obvious jump in Fig. 2.6-2.10 and Fig. 3.8-3.9 when we estimate the orientation order parameters at various density in our Monte Carlo simulation. For $l_p/R = 1$, the transition gap is too small to be shown in Fig. 3.1.

To compare the results from the theoretical analysis with that from computer simulations, we plot the critical values of n from both methods as a function of l_p/R in one figure (Fig. 3.11). The two results show a consistent decrease at high value of l_p/R. The decrease is dominated by the second term in the equilibrium densities (Eqn. 3.19-3.21), which comes from the inhomogeneous spatial distribution of polymer on the spherical surface. However, there are two inconsistent aspects here. The first one is that the simulation presents a proportional line at low density because the bead volume in the bead-rod model plays an important role in the excluded volume. The other one is the critical value of n. The theoretical analysis shows the critical value of n around 3 or 4 times of that from simulations. We think the difference might come from the long-chain assumption within the theoretical derivations (See Appendix C for details), in which we assume that the polymer chain is long enough to cancel the dependence of density distribution on the total contour length of polymer chain in order to make the diffusion-like equation solvable.

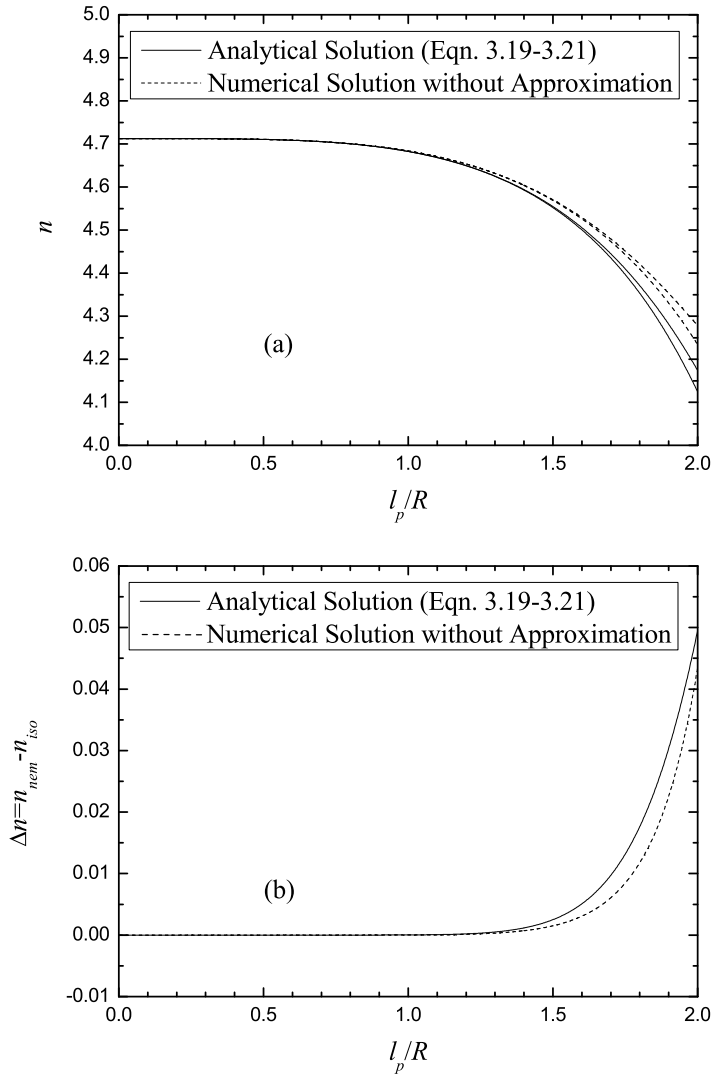

Figure 3.10: The transition gap $n_{hel} = 2\pi v\bar{\varrho}_{hel}$, $n_{iso} = 2\pi v\bar{\varrho}_{iso}$ versus l_p/R, the ratio of the persistence length and the radius of spherical surface

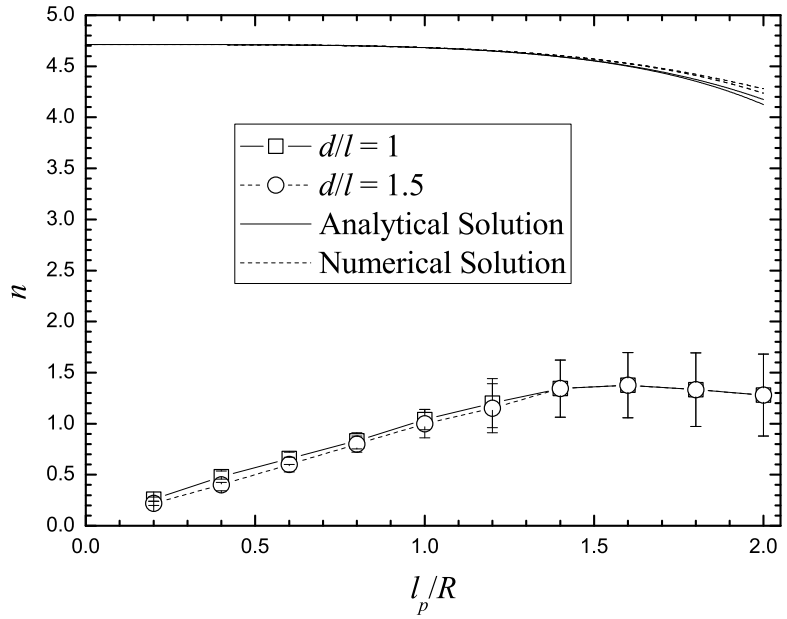

Figure 3.11: The critical value of n obtained from computer simulations and theoretical analysis is plotted as a function of l_p/R, the ratio of the persistence length and the radius of spherical surface.

Chapter 4

Conclusion

We investigated the equilibrium conformations of semiflexible polymer chains confined to a spherical surface by means of both computer simulation and theoretical analysis. Both methods showed a consistent result: the helicoidal state of polymer conformation exists at sufficiently high surface density, while the isotropic state at low density. At the helicoidal phase the segments of polymer chain have more probability to be parallel and close to the equator. For any given l_p/R, the equilibrium conformation is determined by the value of $n = Nl_p^2/4\pi R^2$, which actually represents the ratio of total excluded volume and total space volume, where N is the number of segments, R is the sphere radius and l_p is the persistence length that is related to the excluded volume effect in 2D system. We also estimated the critical value of n for various l_p/R. For polymer on a plane, the critical value of n is constant for arbitrary persistence length. However, the phase transition takes place at lower value of n for the polymer with longer persistence length on a spherical surface. A possible reason is the spherical surface can strengthen the excluded volume interaction relative to the plane. This induces that the critical value of n decreases with longer persistence length as both computer simulation and theoretical analysis showed. In addition, with the phase equilibrium conditions, we analytically figured out the transition gap and indicated that the isotropic-helicoidal phase transition is weak-first-order.

Appendix A

Wiener Integral and Diffusion-like Equation for Polymer Configuration

We follow the reference [12, 8] to compose this appendix.

For getting the Wiener distribution, we consider the equivalent Gaussian chain with the maximum contour length L. The mean square end-end distance of Gaussian chain is proportional to L and we define the ratio as the step length l:

$$l \equiv \frac{< \boldsymbol{R}^2 >}{L} = \text{constant} \tag{A.1}$$

For the chain consisting of n Gaussian links of size Δs, where $n\Delta s \equiv L$, the bond probability is given by the definition of Gaussian chain:

$$\tau\left(\boldsymbol{R}_j\right) = \tau\left(\boldsymbol{r}_j - \boldsymbol{r}_{j-1}\right) = \left(\frac{3}{2\pi l \Delta s}\right)^{3/2} \exp\left(-\frac{3\boldsymbol{R}_j^2}{2l\Delta s}\right) \tag{A.2}$$

where $\boldsymbol{r}_j$ is the position of j-th monomer and $\boldsymbol{R}_j$ is the j-th bond vector. We can get the

probability distribution function as:

$$\begin{aligned} P(\{\boldsymbol{r}_k\}) &= Q^{-1}G(\{\boldsymbol{R}_k\}) = Q^{-1}\prod_{j=1}^{n}\tau\left(\boldsymbol{R}_j\right) \\ &= \prod_{j=1}^{n}\left[\left(\frac{3}{2\pi l\Delta s}\right)^{3/2}\exp\left(-\frac{3\left(\boldsymbol{r}_j-\boldsymbol{r}_{j-1}\right)^2}{2l\Delta s}\right)\right] \\ &= \mathscr{N}\exp\left(-\sum_{j=1}^{n}\frac{3\left(\boldsymbol{r}_j-\boldsymbol{r}_{j-1}\right)^2}{2l\Delta s}\right) \end{aligned} \tag{A.3}$$

where Q is the partition function and $\mathscr{N}$ is the normalization factor that satisfies $\mathscr{N} = (3/2\pi l\Delta s)^{3n/2}$.

Then we take the continuous limit as $\Delta s \to 0$,$n \to \infty$ and fix $n\Delta s = L$ to the exponential in Eqn. A.3, which becomes

$$\lim_{\mathrm{FI}}\sum_{j=1}^{n}\left|\frac{\boldsymbol{r}_j-\boldsymbol{r}_{j-1}}{\Delta s}\right|^2\Delta s = \int_0^L\left|\frac{\partial\boldsymbol{r}(\tau)}{\partial\tau}\right|^2 d\tau = \int_0^L|\dot{\boldsymbol{r}}(\tau)|^2\,d\tau \tag{A.4}$$

where τ is the contour length and the notation $\lim_{\mathrm{FI}}$ stands for the functional integral. So the probability density becomes $P[\boldsymbol{r}(\tau)]\,\delta\boldsymbol{r}(\tau)$, which represents the probability that the chain lies between the continuous space curves $\boldsymbol{r}(\tau)$ and $\boldsymbol{r}(\tau)+\delta\boldsymbol{r}(\tau)$. The normalization factor becomes divergent, which could be absorbed into a single differential for the curve $\boldsymbol{r}(\tau)$:

$$\mathscr{N}\delta\boldsymbol{r}(\tau) = \mathscr{D}[\boldsymbol{r}(\tau)] \tag{A.5}$$

Finally, we get the probability of the chain configuration $\boldsymbol{r}(\tau)$ as

$$P[\boldsymbol{r}(\tau)]\,\delta\boldsymbol{r}(\tau) = \mathscr{D}[\boldsymbol{r}(\tau)]\exp\left(-\frac{3}{2l}\int_0^L|\dot{\boldsymbol{r}}(\tau)|^2\,d\tau\right) \tag{A.6}$$

which is well known as Wiener distribution.

Now, we consider the case of a polymer chain in an external fields to derive the diffusion-like equation for polymer configuration. In addition to Eqn. A.3 the unnormalized thermal distribution function for the discrete chain in an external field is written as

$$G(\{\boldsymbol{r}_k\}) = \exp\left[-\frac{3}{2l\Delta s}\sum_{j=1}^{n}\left|\boldsymbol{r}_j-\boldsymbol{r}_{j-1}\right|^2-\beta\Delta s\sum_{j=1}^{n}W\left(\frac{\boldsymbol{r}_j+\boldsymbol{r}_{j-1}}{2}\right)\right] \tag{A.7}$$

where W is the external field. Because of the presence of the external field, the space is no longer translationally invariant. Define $\boldsymbol{r}_0 = \boldsymbol{R}'$ and $d\{\boldsymbol{r}_k\} = \prod_{j=1}^{n} d\boldsymbol{r}_j$. In the limit of a continuous chain, the second term of Eqn. A.7 becomes

$$\lim_{\mathrm{FI}} \beta\Delta s \sum_{j=1}^{n} W\left(\frac{\boldsymbol{r}_j + \boldsymbol{r}_{j-1}}{2}\right) = \int_0^L V\left[\boldsymbol{r}(\tau)\right] d\tau \tag{A.8}$$

where $V \equiv \beta W$. The expression of unnormalized polymer distribution function in the continuous limit could be written as

$$G\left[\boldsymbol{r}(\tau)\right] \delta\boldsymbol{r}(\tau) = \mathscr{D}\left[\boldsymbol{r}(\tau)\right] \exp\left[-\int_0^L d\tau \left\{\frac{3}{2l}\left|\dot{\boldsymbol{r}}(\tau)\right|^2 + V\left[\boldsymbol{r}(\tau)\right]\right\}\right] \tag{A.9}$$

As mentioned before, we pay attention to the end-end vector probability distribution. The fixed end-vector partition function is

$$\begin{aligned} G(\boldsymbol{R}, \boldsymbol{R}'; L) &= \int \delta\boldsymbol{r}(\tau) \int d\boldsymbol{r}(0) \delta\left[\boldsymbol{r}(0) - \boldsymbol{R}'\right] \delta\left[\boldsymbol{r}(L) - \boldsymbol{R}\right] G\left[\boldsymbol{r}(\tau)\right] \\ &= \int_{\boldsymbol{r}(0)=\boldsymbol{R}'}^{\boldsymbol{r}(L)=\boldsymbol{R}} \mathscr{D}\left[\boldsymbol{r}(\tau)\right] \exp\left[-\int_0^L d\tau \left\{\frac{3}{2l}\left|\dot{\boldsymbol{r}}(\tau)\right|^2 + V\left[\boldsymbol{r}(\tau)\right]\right\}\right] \end{aligned} \tag{A.10}$$

which defines the functional integral for $G(\boldsymbol{R}, \boldsymbol{R}'; L)$.

For $V \equiv 0$, $G(\boldsymbol{R}, \boldsymbol{R}'; L)$ becomes the probability distribution of the end-end vector, which is given by

$$G_0(\boldsymbol{R}, \boldsymbol{R}'; L) = \left(\frac{3}{2\pi l L}\right)^{3/2} \exp\left(-\frac{3(\boldsymbol{R} - \boldsymbol{R}')^2}{2lL}\right) \Theta(L) \tag{A.11}$$

where $\Theta(L)$ is step function.

Unfortunately, in some cases, the expression of $G(\boldsymbol{R}, \boldsymbol{R}'; L)$ in function integral is generally not very useful. So we try to evaluate it by the inverse of differentiation. To derive the differential equation of $G(\boldsymbol{R}, \boldsymbol{R}'; L)$, we use the relationship

$$G(\boldsymbol{R}, \boldsymbol{R}'; L + \Delta L) = \int d\boldsymbol{R}'' G(\boldsymbol{R}, \boldsymbol{R}''; \Delta L) G(\boldsymbol{R}'', \boldsymbol{R}'; L) \tag{A.12}$$

For τ between L and $L + \Delta L$, if V changes little for various $\boldsymbol{r}$, the energy is approximated as

$$\int_L^{L+\Delta L} d\tau V\left[\boldsymbol{r}(\tau)\right] = \Delta L V(\boldsymbol{R}) \tag{A.13}$$

Then, from Eqn. A.10, we can write $G(\boldsymbol{R}, \boldsymbol{R}'; L + \Delta L)$ as

$$G(\boldsymbol{R}, \boldsymbol{R}'; L + \Delta L) = \exp(-\Delta L V(\boldsymbol{R})) \int d\boldsymbol{R}'' G_0(\boldsymbol{R}, \boldsymbol{R}''; \Delta L) G(\boldsymbol{R}'', \boldsymbol{R}'; L) \tag{A.14}$$

For small ΔL, expand $G(\boldsymbol{R}'', \boldsymbol{R}'; L)$ in terms of $\boldsymbol{r} \equiv \boldsymbol{R} - \boldsymbol{R}''$:

$$\begin{aligned}
& \int d\boldsymbol{R}'' G_0(\boldsymbol{R}, \boldsymbol{R}''; \Delta L) G(\boldsymbol{R}'', \boldsymbol{R}'; L) \\
= & \int dr G_0(\boldsymbol{R}, \boldsymbol{R}''; \Delta L) G(\boldsymbol{R} - \boldsymbol{r}, \boldsymbol{R}'; L) \\
= & \int dr G_0(\boldsymbol{R}, \boldsymbol{R}''; \Delta L) \left(1 - \boldsymbol{r} \cdot \frac{\partial}{\partial \boldsymbol{R}} + \frac{1}{2} \boldsymbol{r}\boldsymbol{r} : \frac{\partial^2}{\partial \boldsymbol{R} \partial \boldsymbol{R}}\right) G(\boldsymbol{R}, \boldsymbol{R}'; L) \\
= & \left(1 + \frac{1}{6} \Delta L l \nabla_{\boldsymbol{R}}^2\right) G(\boldsymbol{R}, \boldsymbol{R}'; L)
\end{aligned} \tag{A.15}$$

Thus, to the order of ΔL, Eqn. A.14 should be

$$\left(1 + \Delta L \frac{\partial}{\partial L}\right) G(\boldsymbol{R}, \boldsymbol{R}'; L) = (1 - \Delta L V(\boldsymbol{R})) \left(1 + \frac{1}{6} \Delta L l \nabla_{\boldsymbol{R}}^2\right) G(\boldsymbol{R}, \boldsymbol{R}'; L) \tag{A.16}$$

The differential equation of $G(\boldsymbol{R}, \boldsymbol{R}'; L)$ can be obtained by collecting all the terms of order ΔL:

$$\left(\frac{\partial}{\partial L} - \frac{l}{6} \nabla_{\boldsymbol{R}}^2 + V(\boldsymbol{R})\right) G(\boldsymbol{R}, \boldsymbol{R}'; L) = 0 \tag{A.17}$$

This equation holds for $L > 0$. With the definition of $G(\boldsymbol{R}, \boldsymbol{R}'; L) = 0$ for $L < 0$ and the boundary condition that $\lim_{L \to 0} G(\boldsymbol{R}, \boldsymbol{R}'; L) = \delta(\boldsymbol{R} - \boldsymbol{R}')$, the diffusion-like equation for the flexible polymer chain in the presence of an external field can be described as:

$$\left(\frac{\partial}{\partial L} - \frac{l}{6} \nabla_{\boldsymbol{R}}^2 + V(\boldsymbol{R})\right) G(\boldsymbol{R}, \boldsymbol{R}'; L) = \delta(L) \delta(\boldsymbol{R} - \boldsymbol{R}') \tag{A.18}$$

$G(\boldsymbol{R}, \boldsymbol{R}'; L)$ is then the Green's function for the diffusion-like equation with the diffusion constant $D = l/6$. The diffusion-like equation illuminates an analogy between the configuration of continuous equivalent chain and the path of a particle undergoing Brownian or diffusive motion.

Appendix B

Diffusion-like Equation of Semiflexible Polymer Chains

We follow the reference [12, 11] to compose this appendix.

We first consider a polymer chain with stiffness in the absence of external field. Define the tangent vector

$$\boldsymbol{u}(\tau) = \dot{\boldsymbol{r}}(\tau) = \frac{d\boldsymbol{r}(\tau)}{d\tau} \tag{B.1}$$

As STY [28] discussed, in the case of polymer chains with stiffness, we introduce a bending energy, which is given by

$$V_B = \frac{1}{2}\varepsilon \int_0^L \left| \frac{\partial \boldsymbol{u}(\tau)}{\partial \tau} \right|^2 d\tau = \frac{1}{2}\varepsilon \int_0^L |\ddot{\boldsymbol{r}}(\tau)|^2 \, d\tau \tag{B.2}$$

where ε is called bending penalty in this thesis. Then, the unnormalized distribution function is

$$G(\boldsymbol{R}, \boldsymbol{R}'; L) = \int_{r(0)=\boldsymbol{R}'}^{r(L)=\boldsymbol{R}} \mathscr{D}[\boldsymbol{r}(\tau)] \exp\left[- \int_0^L d\tau \left\{ \frac{3}{2l} |\dot{\boldsymbol{r}}(\tau)|^2 + \frac{1}{2}\beta\varepsilon |\ddot{\boldsymbol{r}}(\tau)|^2 \right\} \right] \tag{B.3}$$

Substituting Eqn. B.1, changing the normalization and setting $\boldsymbol{r}(0) = \boldsymbol{R}' = 0$ (because of the spatial translational invariant), we can also describe $G(\boldsymbol{R}, \boldsymbol{R}'; L)$ in Eqn. B.3 in terms

of tangent vectors as

$$\begin{aligned} & G\left(\boldsymbol{R}, \boldsymbol{U}\boldsymbol{U}'; L\right) \\ = & \int_{\boldsymbol{u}(0)=\boldsymbol{U}'}^{\boldsymbol{u}(L)=\boldsymbol{U}} \left\{ \mathscr{D}\left[\boldsymbol{u}\left(\tau\right)\right] \delta\left[\boldsymbol{R} - \int_0^L \boldsymbol{u}\left(\tau\right) d\tau\right] \right. \\ & \left. \exp\left[- \int_0^L d\tau \left(\frac{3}{2l} \left|\boldsymbol{u}\left(\tau\right)\right|^2 + \frac{1}{2}\beta\varepsilon \left|\dot{\boldsymbol{u}}\left(\tau\right)\right|^2 \right) \right] \right\} \end{aligned} \tag{B.4}$$

Then, to derive the partial differential equation for $G\left(\boldsymbol{R}, \boldsymbol{U}\boldsymbol{U}'; L\right)$, apply Fourier transform to the Dirac delta function in Eqn. B.4:

$$\delta\left[\boldsymbol{R} - \int_0^L \boldsymbol{u}\left(\tau\right) d\tau\right] = \int \frac{d^3k}{\left(2\pi\right)^3} \exp\left\{ -i\boldsymbol{k} \cdot \left[\boldsymbol{R} - \int_0^L \boldsymbol{u}\left(\tau\right) d\tau\right] \right\} \tag{B.5}$$

Define $I\left(\boldsymbol{k}, \boldsymbol{U}\boldsymbol{U}'; L\right)$ as:

$$\begin{aligned} & I\left(\boldsymbol{k}, \boldsymbol{U}\boldsymbol{U}'; L\right) \\ = & \int_{\boldsymbol{u}(0)=\boldsymbol{U}'}^{\boldsymbol{u}(L)=\boldsymbol{U}} \mathscr{D}\left[\boldsymbol{u}\left(\tau\right)\right] \exp\left[- \int_0^L d\tau \left\{ \frac{3}{2l} \left|\boldsymbol{u}\left(\tau\right)\right|^2 + \frac{1}{2}\beta\varepsilon \left|\dot{\boldsymbol{u}}\left(\tau\right)\right|^2 - i\boldsymbol{k} \cdot \boldsymbol{u}\left(\tau\right) \right\} \right] \end{aligned} \tag{B.6}$$

So the equation B.4 could be rewritten as

$$G\left(\boldsymbol{R}, \boldsymbol{U}\boldsymbol{U}'; L\right) = \int \frac{d^3k}{\left(2\pi\right)^3} \exp\left(-i\boldsymbol{k} \cdot \boldsymbol{R}\right) I\left(\boldsymbol{k}, \boldsymbol{U}\boldsymbol{U}'; L\right) \tag{B.7}$$

where $I\left(\boldsymbol{k}, \boldsymbol{U}\boldsymbol{U}'; L\right)$ satisfies the diffusion-like equation:

$$\left(\frac{\partial}{\partial L} - \frac{1}{2\beta\varepsilon} \nabla_U^2 + \frac{3}{2l} \boldsymbol{U}^2 - i\boldsymbol{k} \cdot \boldsymbol{U} \right) I\left(\boldsymbol{k}, \boldsymbol{U}\boldsymbol{U}'; L\right) = \delta\left(L\right) \delta\left(\boldsymbol{U} - \boldsymbol{U}'\right) \tag{B.8}$$

Thus, we could write the differential equation by using the Fourier transform B.7:

$$\left(\frac{\partial}{\partial L} - \frac{1}{2\beta\varepsilon} \nabla_U^2 + \frac{3}{2l} \boldsymbol{U}^2 + \boldsymbol{U} \cdot \nabla_{\boldsymbol{R}} \right) G\left(\boldsymbol{R}, \boldsymbol{U}\boldsymbol{U}'; L\right) = \delta\left(L\right) \delta\left(\boldsymbol{R}\right) \delta\left(\boldsymbol{U} - \boldsymbol{U}'\right) \tag{B.9}$$

This is the diffusion-like equation for the polymer with stiffness in the absence of external field.

Appendix C

Derivation for the Landau Expansion of Free Energy for a Wormlike Chain Confined to a Spherical Surface

In this appendix we introduce the derivation for the Landau expansion of free energy for a wormlike chain confined to a spherical surface. First we define the partition function $q(\boldsymbol{R}, \boldsymbol{U}; L)$ for the unnormalized probability distribution $G(\boldsymbol{R}\boldsymbol{R}', \boldsymbol{U}\boldsymbol{U}'; L)$ as

$$q(\boldsymbol{R}, \boldsymbol{U}; L) = \iint d\boldsymbol{R}' d\boldsymbol{U}' G(\boldsymbol{R}\boldsymbol{R}', \boldsymbol{U}\boldsymbol{U}'; L) \tag{C.1}$$

which represents the probability for a polymer chain with the total contour length L ending at the position $\boldsymbol{r}$ and with the end vector $\boldsymbol{u}$. With the diffusion-like equation of polymer in external fields and polymer with stiffness in Appendix A and B respectively, we could write the diffusion-like equation for the partition function of semiflexible polymer for $L > 0$ involving the main idea of self-consistent field:

$$\left[l_p \frac{\partial}{\partial L} - \nabla_{\boldsymbol{U}}^2 + l_p \boldsymbol{U} \cdot \nabla_{\boldsymbol{R}} + w(\boldsymbol{R}, \boldsymbol{U}) \right] q(\boldsymbol{R}, \boldsymbol{U}; L) = 0 \tag{C.2}$$

Here the constant term ($|\boldsymbol{U}| \equiv 1$) in the differential operator has been absorbed into the dimensionless mean field term $w(\boldsymbol{R}, \boldsymbol{U})$ and l_p is the persistence length, which is written by $l_p = 2\beta\varepsilon$ for the 2 dimensional system as mentioned in Chapter 1.

For a long chain, q is L-independent. So the diffusion-like equation C.2 can be rewritten as:

$$\left[\nabla_U^2 - l_p \boldsymbol{U} \cdot \nabla_{\boldsymbol{R}}\right] q(\boldsymbol{R}, \boldsymbol{U}) = w(\boldsymbol{R}, \boldsymbol{U})\, q(\boldsymbol{R}, \boldsymbol{U}) \tag{C.3}$$

The partition function $q(\boldsymbol{R}, \boldsymbol{U})$ corresponds to the probability of finding the polymer chain ending at the position $\boldsymbol{R}$ with the unit end-vector $\boldsymbol{U}$. To avoid the confusion with R, the radius of the spherical surface, we rewrite the notation $\boldsymbol{R}$ and $\boldsymbol{U}$ to lower cases $\boldsymbol{r}$ and $\boldsymbol{u}$.

Any segment along the chain could be treated as two ends adjoined with opposite directions. So there is a relationship between the density distribution ρ of polymer chain and the partition function q:

$$\rho(\boldsymbol{r}, \boldsymbol{u}) = q(\boldsymbol{r}, -\boldsymbol{u}) q(\boldsymbol{r}, \boldsymbol{u}) \tag{C.4}$$

We call this relation as jointing equation. And the density distribution ρ satisfies $\int \rho d\boldsymbol{r} d\boldsymbol{u} = N$, where N is the total number of segments. And the average density is defined as $\varrho = N/4\pi R^2$.

For a polymer chain confined to a spherical surface, because of the fixed R, the radius of the sphere, and the axial symmetry, the segment position $\boldsymbol{r}$ on the sphere can be described only by the latitude Θ. The tangent vector $\boldsymbol{u}$, which contains only one freedom degree, can be described by θ that is the angle between $\boldsymbol{u}$ and the azimuthal direction $\hat{\boldsymbol{\Phi}}$ (See Fig. 1.5). Thus, all of q, ρ and w are the functions of Θ and θ. The symmetry conditions can be expressed by:

$$q(\Theta, \theta) = q(\Theta, \pi - \theta) \tag{C.5}$$

$$q(\Theta, \theta) = q(\pi - \Theta, \pi + \theta) \tag{C.6}$$

Besides these, ρ and w have one more, because ρ and w don't distinguish the tangent vector with its opposite one:

$$\rho(\Theta, \theta) = \rho(\Theta, \pi + \theta) \tag{C.7}$$

$$w(\Theta, \theta) = w(\Theta, \pi + \theta) \tag{C.8}$$

One could expand ρ, q and w in the basis functions $P_l(\cos\Theta)\, e^{im'\theta}$, which is reduced from the multiply of the two spherical harmonics $Y_{lm}(\Theta, \Phi)\, Y_{l'm'}(\vartheta, \theta)$, and keep the surviving

terms according to the symmetry conditions:

$$\begin{aligned} q(\Theta,\theta) &= q_{00} + q_{02}\cos 2\theta + q_{11}P_1(\cos\Theta)\sin\theta + q_{20}P_2(\cos\Theta) \\ &\quad + q_{04}\cos 4\theta + q_{13}P_1(\cos\Theta)\sin 3\theta + q_{22}P_2(\cos\Theta)\cos 2\theta \\ &\quad + q_{31}P_3(\cos\Theta)\sin\theta + q_{40}P_4(\cos\Theta) + \cdots \end{aligned} \tag{C.9}$$

$$\begin{aligned} \rho(\Theta,\theta) &= \rho_{00} + \rho_{02}\cos 2\theta + \rho_{20}P_2(\cos\Theta) \\ &\quad + \rho_{04}\cos 4\theta + \rho_{22}P_2(\cos\Theta)\cos 2\theta + \rho_{40}P_4(\cos\Theta) + \cdots \end{aligned} \tag{C.10}$$

$$\begin{aligned} w(\Theta,\theta) &= w_{02}\cos 2\theta + w_{20}P_2(\cos\Theta) \\ &\quad + w_{04}\cos 4\theta + w_{22}P_2(\cos\Theta)\cos 2\theta + w_{40}P_4(\cos\Theta) + \cdots \end{aligned} \tag{C.11}$$

Because the differential operator in the left-hand side of the diffusion-like equation (Eqn. C.3) does not contain any constant term, there is no constant term in the expansion of w either.

In the coordinates of θ and Θ, the diffusion-like equation (Eqn. C.3) becomes

$$\left[\frac{\partial^2}{\partial\theta^2} + \frac{l_p}{R}\sin\theta\frac{\partial}{\partial\Theta}\right] q(\Theta,\theta) = w(\Theta,\theta)\, q(\Theta,\theta) \tag{C.12}$$

And the constant term of the expansions of q and ρ can be normalized as:

$$\begin{aligned} \psi(\Theta,\theta) &= q(\Theta,\theta)/q_{00} \\ &= 1 + \psi_{02}\cos 2\theta + \psi_{11}P_1(\cos\Theta)\sin\theta + \psi_{20}P_2(\cos\Theta) \\ &\quad + \psi_{04}\cos 4\theta + \psi_{13}P_1(\cos\Theta)\sin 3\theta + \psi_{22}P_2(\cos\Theta)\cos 2\theta \\ &\quad + \psi_{31}P_3(\cos\Theta)\sin\theta + \psi_{40}P_4(\cos\Theta) + \cdots \end{aligned} \tag{C.13}$$

$$\begin{aligned} \phi(\Theta,\theta) &= \rho(\Theta,\theta)/\rho_{00} \\ &= 1 + \phi_{02}\cos 2\theta + \phi_{20}P_2(\cos\Theta) \\ &\quad + \phi_{04}\cos 4\theta + \phi_{22}P_2(\cos\Theta)\cos 2\theta + \phi_{40}P_4(\cos\Theta) + \cdots \end{aligned} \tag{C.14}$$

ρ_{00} is proportional to the averaged surface density of polymer segments, i.e. $\rho_{00} = \varrho/2\pi$. For convenience, we define the reduced surface density as $\bar{\varrho} = \rho_{00} = \varrho/2\pi$ and the orientational and spatial order parameters as:

$$\sigma = <\cos 2\theta> = \frac{\iint \cos 2\theta\phi(\Theta,\theta)\sin\Theta d\Theta d\theta}{\iint \phi(\Theta,\theta)\sin\Theta d\Theta d\theta} = \frac{\phi_{02}}{2} = \frac{\rho_{02}}{2\rho_{00}} \tag{C.15}$$

$$\eta = <P_2(\cos\Theta)> = \frac{\iint P_2(\cos\Theta)\phi(\Theta,\theta)\sin\Theta d\Theta d\theta}{\iint \phi(\Theta,\theta)\sin\Theta d\Theta d\theta} = \frac{\phi_{20}}{5} = \frac{\rho_{20}}{5\rho_{00}} \tag{C.16}$$

which are the same definitions in Chapter 1 (See Eqn. 1.5 and 1.6).

By combining the diffusion-like equation (C.12) and jointing equation (C.4), the coefficients of w can be expressed in terms of those of ϕ. Because the differential operator in the left-hand side of the diffusion-like equation (C.12) is not diagonal in the representation of the bases $P_n(\cos\Theta)\, e^{im\theta}$, the coefficients of ϕ are in the same order of each other when operating the minimization of free energy. It is a little difficult to cut off the expansions of ϕ, ψ and w. However, fortunately, the coupling between ϕ_{02}, which represents the order parameter we concern about, and another coefficient ϕ_{nm} becomes weaker and weaker with a greater n for $m \neq 2$. We use trial expansions, which are cut off to the "fourth order" terms (See Eqn. C.9-C.14), to obtain the relations as following:

$$w_{02} = -4\psi_{02} + \frac{\alpha}{8}\psi_{11} - \frac{\alpha}{8}\psi_{13} + \frac{3\alpha}{64}\psi_{31} + \mathscr{O}\left(\psi_{02}^2\right) \tag{C.17}$$

$$w_{20} = \frac{5\alpha}{64}\psi_{11} - \frac{105\alpha}{256}\psi_{31} + \mathscr{O}\left(\psi_{20}^2\right) \tag{C.18}$$

$$w_{04} = -16\psi_{04} + \frac{\alpha}{8}\psi_{13} + \mathscr{O}\left(\psi_{04}^2\right) \tag{C.19}$$

$$w_{22} = -4\psi_{22} - \frac{5\alpha}{64}\psi_{11} + \frac{5\alpha}{64}\psi_{13} + \frac{105\alpha}{256}\psi_{31} + \mathscr{O}\left(\psi_{22}^2\right) \tag{C.20}$$

$$w_{40} = \frac{9\alpha}{256}\psi_{11} + \frac{2079\alpha}{8192}\psi_{31} + \mathscr{O}\left(\psi_{40}^2\right) \tag{C.21}$$

$$\psi_{11} = -\frac{9\alpha}{16}\psi_{20} + \frac{9\alpha}{32}\psi_{22} - \frac{15\alpha}{64}\psi_{40} + \mathscr{O}\left(\psi_{20}^2\right) \tag{C.22}$$

$$\psi_{13} = -\frac{\alpha}{32}\psi_{22} + \mathscr{O}\left(\psi_{22}^2\right) \tag{C.23}$$

$$\psi_{31} = \frac{21\alpha}{64}\psi_{20} - \frac{21\alpha}{128}\psi_{22} - \frac{1085\alpha}{1024}\psi_{40} + \mathscr{O}\left(\psi_{20}^2\right) \tag{C.24}$$

$$\psi_{02} = \frac{1}{2}\phi_{02} + \mathscr{O}\left(\phi_{02}^2\right) \tag{C.25}$$

$$\psi_{20} = \frac{1}{2}\phi_{20} + \mathscr{O}\left(\phi_{20}^2\right) \tag{C.26}$$

$$\psi_{04} = \frac{1}{2}\phi_{04} + \mathscr{O}\left(\phi_{04}^2\right) \tag{C.27}$$

$$\psi_{22} = \frac{1}{2}\phi_{22} + \mathscr{O}\left(\phi_{22}^2\right) \tag{C.28}$$

$$\psi_{40} = \frac{1}{2}\phi_{40} + \mathscr{O}\left(\phi_{40}^2\right) \tag{C.29}$$

where $\alpha = \pi l_p / R$ and only first order terms are kept to ensure that the Landau expansion

of reduced free energy $\tilde{F}$ contains all of second order terms, which is defined as:

$$\tilde{F} = \frac{\beta F}{\iint d\boldsymbol{r}d\boldsymbol{u}} = \frac{\beta F}{8\pi^2 R^2} \tag{C.30}$$

The coefficient in front of the ϕ_{02}^2 term is $\left(\frac{1}{2} - \frac{2}{3}v\bar{\varrho}\right)\bar{\varrho}$, which determines the critical density for the order parameter ϕ_{02} is around $\bar{\varrho} = 3/4v$. With the minimization conditions $\partial\tilde{F}/\partial\phi_{ij} = 0$ and $\partial^2\tilde{F}/\partial\phi_{ij}^2 > 0$, the leading term of the coupling between coefficients for the segmental density in the region near the critical point $3/4v$ could be obtained: $\phi_{20} \approx 10^{-2}\phi_{02}$, $\phi_{40} \approx 10^{-2}\phi_{20}$ and $\phi_{04} \approx 10^{-3}\phi_{22}$. The critical density for ϕ_{22} is very close to that of ϕ_{02} because of the common factor $\cos 2\theta$. Therefore, the coefficients ϕ_{n2} with any n are in the same order. And the terms of $P_n(\cos\Theta)\cos m\theta$ with any n for $m \geq 4$ and with $n \geq 4$ for $m = 0$ could be neglected. In this case, we keep $P_2(\cos\Theta)$ to involve the spatial distribution on the spherical surface and also keep the terms with any n for $m = 2$. The expansion of ϕ could be rewritten as:

$$\begin{aligned}\phi(\Theta,\theta) \approx\ & 1 + [\phi_{02} + \phi_{22}P_2(\cos\Theta) + \phi_{42}P_4(\cos\Theta) \\ & + \phi_{62}P_6(\cos\Theta) + \phi_{82}P_8(\cos\Theta) + \cdots]\cos 2\theta + \phi_{20}P_2(\cos\Theta)\end{aligned} \tag{C.31}$$

Here we collected more terms in the square bracket above and got more accurate relations: $\phi_{22} \approx 0.645\phi_{02}$, $\phi_{42} \approx 0.305\phi_{02}$, $\phi_{62} \approx 0.214\phi_{02}$, $\phi_{82} \approx 0.190\phi_{02}$, etc. Combined with the weight function $\sin\Theta$ for the Legendre polynomials, the probability density distribution function $\phi_{02} + \phi_{22}P_2(\cos\Theta) + \phi_{42}P_4(\cos\Theta) + \phi_{62}P_6(\cos\Theta) + \phi_{82}P_8(\cos\Theta) + \cdots$ approaches to be uniform asymptotically along with more terms considered. Thus, we set the expansions to be cut off to "second order" terms, i.e.

$$\begin{aligned}\psi(\Theta,\theta) &= q(\Theta,\theta)/q_{00} \\ &\approx 1 + \psi_{02}\cos 2\theta + \psi_{11}P_1(\cos\Theta)\sin\theta + \psi_{20}P_2(\cos\Theta) \qquad \text{(C.32)} \\ \phi(\Theta,\theta) &= \rho(\Theta,\theta)/\rho_{00} \\ &\approx 1 + \phi_{02}\cos 2\theta + \phi_{20}P_2(\cos\Theta) \qquad \text{(C.33)} \\ w(\Theta,\theta) &\approx w_{02}\cos 2\theta + w_{20}P_2(\cos\Theta)\end{aligned}$$

With these expansions we derive the relationship between the coefficients of ϕ, ψ and w

again:

$$w_{02} = -4\psi_{02} + \frac{\alpha}{8}\psi_{11} \tag{C.34}$$

$$w_{20} = \frac{5\alpha}{64}\psi_{11} \tag{C.35}$$

$$\psi_{11} = -\frac{9\alpha}{16}\psi_{20} \tag{C.36}$$

$$q_{00}^2 = \rho_{00}\left(1 - \frac{1}{8}\phi_{02}^2 - \frac{1}{20}\phi_{20}^2 + \frac{27\alpha^2}{2048}\phi_{20}^2\right) \tag{C.37}$$

$$\psi_{02} = \frac{1}{2}\phi_{02}\left(1 + \frac{1}{8}\phi_{02}^2 + \frac{1}{20}\phi_{20}^2 - \frac{27\alpha^2}{2048}\phi_{20}^2\right) - \frac{27\alpha^2}{4096}\phi_{20}^2 \tag{C.38}$$

$$\psi_{20} = \frac{1}{2}\phi_{20}\left(1 + \frac{1}{8}\phi_{02}^2 + \frac{1}{20}\phi_{20}^2 - \frac{27\alpha^2}{2048}\phi_{20}^2\right) - \frac{1}{28}\phi_{20}^2 + \frac{27\alpha^2}{2048}\phi_{20}^2 \tag{C.39}$$

Then the Landau expansion of free energy in terms of both orientational and spatial order parameters with the relationship $\sigma = \phi_{02}/2$ and $\eta = \phi_{20}/5$ can be expressed as:

$$\begin{aligned}
\tilde{F} = {} & 4v\bar{\varrho}^2 + \left(2 - \frac{8}{3}v\bar{\varrho}\right)\bar{\varrho}\sigma^2 + \frac{45}{512}\alpha^2\bar{\varrho}\sigma\eta + \left(\frac{225}{4096}\alpha^2 + 20v\bar{\varrho}\right)\bar{\varrho}\eta^2 \\
& - \left(\frac{2475}{3584}\alpha^2 - \frac{6075}{524288}\alpha^4\right)\bar{\varrho}\sigma\eta^2 - \frac{1125}{28672}\alpha^2\bar{\varrho}\eta^3 \\
& + \bar{\varrho}\sigma^4 + \frac{45}{1024}\alpha^2\bar{\varrho}\sigma^3\eta + \left(\frac{5}{2} - \frac{5175}{8192}\alpha^2\right)\bar{\varrho}\sigma^2\eta^2 \\
& + \left(\frac{225}{2048}\alpha^2 - \frac{30375}{1048576}\alpha^4\right)\bar{\varrho}\sigma\eta^3 \\
& + \left(\frac{30375}{401408}\alpha^2 + \frac{151875}{4194304}\alpha^4 - \frac{4100625}{4294967296}\alpha^6\right)\bar{\varrho}\eta^4 + \cdots
\end{aligned} \tag{C.40}$$

Appendix D

List of Symbols

Symbol	Description
R	Radius of spherical surface
d	Diameter of beads in bead-rod model
l_p	Persistence length for a semiflexible polymer chain
l	Bond length in bead-rod model
L	Total contour length of polymer chain
N	Number of segments of polymer chain
N_b	Number of bonds in the bead-rod model
ε	Bending penalty of the bending energy
σ	Orientational order parameter
η	Spatial order parameter
$\boldsymbol{r}$	Position of a polymer segment
$\boldsymbol{u}$	Tangent vector of polymer chain
τ	Contour length of polymer chain
ρ	Surface density of bonds in bead-rod model
v	Excluded volume per segment
$\rho(\boldsymbol{r}, \boldsymbol{u})$	Density distribution of polymer chain
ϱ	Averaged segmental density on spherical surface
n	Ratio of total excluded volume and total space volume

Bibliography

[1] M. Allen and D. Tildesley. *Computer Simulation of Liquids*. Claredon, Oxford, 1987.

[2] A. Baumgärtner. *Topics in Current Physics*, 36:145, 1984.

[3] C. G. Broyden. *Mathmetics of Computation*, 24:365, 1970.

[4] J. J. Cerda, T. Sintes, and A. Chakrabarti. *Macromolecules*, 38:1469, 2005.

[5] M. E. Cerritelli, N. Cheng, A. H. Rosenborg, C. E. McPherson, F. P. Booy, and A. C. Steven. *Cell*, 91:271, 1997.

[6] Z. Y. Chen. *Phys. Rev. Lett.*, 71:93, 1993.

[7] Z. Y. Chen. *Macromolecules*, 26:3419, 1993.

[8] M. Doi and S. F. Edwards. *The Theory of Polymer Dynamics*. Claredon, Oxford, 1986.

[9] W. C. Earnshaw and S. C. Harrison. *Nature*, 268:598, 1977.

[10] A. Evilevitch, M. C. Castelnovo, M. Knobler, and W. M. Gelbart. *Proc. Natl. Acad. Sci.*, 100:9292, 2003.

[11] K. F. Freed. *Advances in Chemical Physics*, XXII:1, 1972.

[12] K. F. Freed. *Renormalization Group Theory of Macromolecules*. John Wiley & Sons, New York, NY, 1987.

[13] P. Gutjahr, R. Lipowsky, and J. Kierfeld. *Europhys. Lett.*, 76:994, 2006.

[14] J. Kindt, S. Tzlil, A. Ben-Shaul, and W. Gelbart. *Proc. Natl. Acad. Sci.*, 98:13671, 2001.

[15] R. D. Kornberg. *Science*, 184:868, 1974.

[16] K.-K. Kunze and R. R. Netz. *Phys. Rev. Lett.*, 85:4398, 2000.

[17] L. D. Landau and E. M. Lifshitz. *Statistical Physics*. Pergamon, London, U. K., 1969.

[18] C.-H. Lin, Y.-C. Tsai, and C.-K. Hu. *Phys. Rev. E*, 75:031903, 2007.

[19] D. C. Liu and J. Nocedal. *Mathematical Programming B*, 45:503, 1989.

[20] K. Luger, A. W. Mäder, R. K. Richmond, D. F. Sargent, and T. J. Richmond. *Nature*, 389:251, 1997.

[21] T. Odijk. *Macromolecules*, 16:1340, 1983.

[22] A. L. Olins and D. E. Olins. *Science*, 183:330, 1974.

[23] N. H. Olson, M. Gingery, F. A. Eiserling, and T. S. Baker. *Virology*, 279:385, 2001.

[24] L. Onsager. *Ann. N.Y. Acd. Sci.*, 51:627, 1949.

[25] P. K. Purohit, M. M. Inamdar, P. D. Grayson, T. M. Squires, J. Kondev, and R. Phillips. *Biophysical Journal*, 88:851, 2005.

[26] K. E. Richards, R. C. Williams, and R. Calendar. *J. Mol. Biol.*, 78:255, 1973.

[27] T. J. Richmod and C. A. Davey. *Nature*, 423:145, 2003.

[28] N. Saitô, K. Takahashi, and Y. Yunoki. *J. Phys. Soc. (Japan)*, 22:219, 1967.

[29] D. E. Smith, S. J. Tans, S. B. Smith, S. Grimes, D. L. Anderson, and C. Bustamante. *Nature*, 413:748, 2001.

[30] A. J. Spakowitz and Z.-G. Wang. *Phys. Rev. Lett.*, 91:166102, 2003.

[31] Y. Tao, N. H. Olson, W. Xu, D. L. Anderson, M. G. Rossmann, and T. S. Baker. *Cell*, 95:431, 1998.

[32] G. J. Vroege and T. Odijk. *Macromolecules*, 21:2848, 1988.

[33] T. D. Yager, C. T. McMurray, and K. E. van Holde. *Biochemistry*, 28:2271, 1989.

[34] H. Yamakawa. *Modern Theory of Polymer Solutions*. Harper & Row, New York, NY, 1987.

[35] Z. X. Zhang, B. Greene, P. A. Thuman-Commike, J. Jakana, P. E. Prevelige, J. King, and W. Chiu. *J. Mol. Biol.*, 297:615, 2000.